Cell Reports

Myosin VI Drives Clathrin-Mediated AMPA Receptor Endocytosis to Facilitate Cerebellar Long-Term Depression

Graphical Abstract

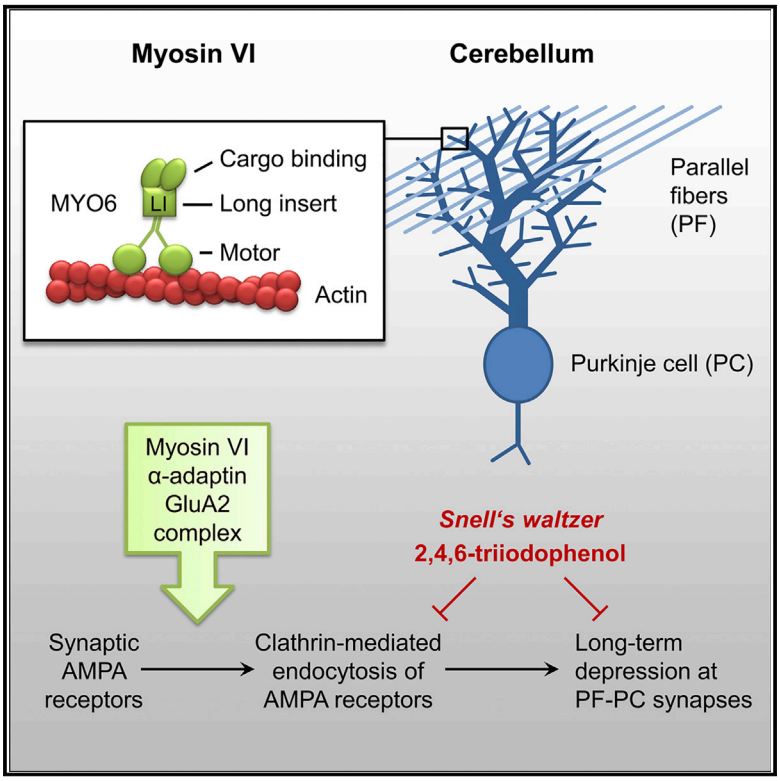

Highlights

- MYO6 is present at cerebellar parallel fiber-Purkinje cell synapses
- Parallel fiber-Purkinje cell LTD is impaired in *Snell's waltzer* and by MYO6 inhibitor
- MYO6 mediates removal of surface AMPA receptors from Purkinje cell spines during LTD
- MYO6 interaction with clathrin adaptor component α-adaptin increases during LTD

Authors

Wolfgang Wagner, Kristina Lippmann, Frank F. Heisler, ..., Jürgen R. Schwarz, Jens Eilers, Matthias Kneussel

Correspondence

wolfgang.wagner@zmnh.uni-hamburg.de (W.W.), matthias.kneussel@zmnh.uni-hamburg.de (M.K.)

In Brief

Wagner et al. investigate the cellular mechanisms that underlie synaptic plasticity in neurons and find that the actin-based cytoskeletal motor myosin VI is directly required for activity-induced, clathrin-mediated endocytosis of AMPA receptors in cerebellar Purkinje cells and for synaptic long-term depression at parallel fiber-Purkinje cell synapses.

Wagner et al., 2019, Cell Reports *28*, 11–20
July 2, 2019
https://doi.org/10.1016/j.celrep.2019.06.005

CellPress

Cell Reports
Report

Myosin VI Drives Clathrin-Mediated AMPA Receptor Endocytosis to Facilitate Cerebellar Long-Term Depression

Wolfgang Wagner,[1,6,*] Kristina Lippmann,[2,6] Frank F. Heisler,[1] Kira V. Gromova,[1] Franco L. Lombino,[1] Mona K. Roesler,[1] Yvonne Pechmann,[1] Sönke Hornig,[1] Michaela Schweizer,[3] Simona Polo,[4,5] Jürgen R. Schwarz,[1] Jens Eilers,[2] and Matthias Kneussel[1,7,*]

[1]Department of Molecular Neurogenetics, Center for Molecular Neurobiology (ZMNH), University Medical Center Hamburg-Eppendorf, 20251 Hamburg, Germany
[2]Carl Ludwig Institute for Physiology, Medical Faculty, University of Leipzig, 04103 Leipzig, Germany
[3]Electron Microscopy Unit, Center for Molecular Neurobiology (ZMNH), University Medical Center Hamburg-Eppendorf, 20251 Hamburg, Germany
[4]Fondazione Istituto FIRC di Oncologia Molecolare (IFOM), 20139 Milan, Italy
[5]Dipartimento di Oncologia ed Emato-oncologia, Università degli Studi di Milano, 20122 Milan, Italy
[6]These authors contributed equally
[7]Lead Contact
*Correspondence: wolfgang.wagner@zmnh.uni-hamburg.de (W.W.), matthias.kneussel@zmnh.uni-hamburg.de (M.K.)
https://doi.org/10.1016/j.celrep.2019.06.005

SUMMARY

Myosin VI is an actin-based cytoskeletal motor implicated in various steps of membrane trafficking. Here, we investigated whether this myosin is crucial for synaptic function and plasticity in neurons. We find that myosin VI localizes at cerebellar parallel fiber to Purkinje cell synapses and that the myosin is indispensable for long-term depression of AMPA-receptor-mediated synaptic signal transmission at this synapse. Moreover, direct visualization of GluA2-containing AMPA receptors in Purkinje cells reveals that the myosin drives removal of AMPA receptors from the surface of dendritic spines in an activity-dependent manner. Co-immunoprecipitation and super-resolution microscopy indicate that specifically the interaction of myosin VI with the clathrin adaptor component α-adaptin is important during long-term depression. Together, these data suggest that myosin VI directly promotes clathrin-mediated endocytosis of AMPA receptors in Purkinje cells to mediate cerebellar long-term depression. Our results provide insights into myosin VI function and the molecular mechanisms underlying synaptic plasticity.

INTRODUCTION

Synaptic plasticity, such as long-term potentiation (LTP) and long-term depression (LTD), is thought to underlie learning and memory. A major way in which such long-lasting changes in synaptic strength are achieved is via varying the number of AMPA receptors (AMPARs) at excitatory synapses (Choquet and Triller, 2013; Kneussel and Hausrat, 2016). Regulated AMPAR trafficking along exo- and endocytic pathways facilitates the modulation of synaptic receptor numbers. Notably, clathrin-mediated endocytosis (CME) of the GluA2 subunit of AMPARs is needed for the downregulation of synaptic AMPARs following stimulation and thus for LTD (Man et al., 2000; Wang and Linden, 2000). Nevertheless, a complete picture of the molecular machinery that mediates LTD-related receptor trafficking is still missing.

Myosins are actin-based cytoskeletal motor proteins, some of which play important roles at synapses (Kneussel and Wagner, 2013; Wagner et al., 2011a). Myosin VI, a unique myosin that moves toward the minus end of the actin filament (Spudich and Sivaramakrishnan, 2010; Wells et al., 1999), is a candidate for regulating postsynaptic function (Heisler et al., 2011; Kneussel and Wagner, 2013). It acts in various steps of membrane trafficking, including CME (Buss et al., 2001; Spudich et al., 2007; Wollscheid et al., 2016), endocytic vesicle transport (Aschenbrenner et al., 2004), and secretion (Tomatis et al., 2013). Myosin VI may also affect actin organization (Isaji et al., 2011; Majewski et al., 2012; Masters et al., 2017).

In brain, myosin VI is present in complex with AMPAR subunits GluA1 and GluA2, the scaffold proteins βSAP97 and GRIP1, as well as the endocytic clathrin machinery (Lv et al., 2015; Osterweil et al., 2005; Wu et al., 2002). Both βSAP97 and GRIP1 might provide a physical link between AMPARs and myosin VI. βSAP97 directly interacts with the C-terminal tail of GluA1 and with the cargo-binding domain (CBD) of the myosin VI heavy chain, MYO6 (Wu et al., 2002). In contrast, GRIP1 directly interacts with GluA2 and with MYO6 (Lv et al., 2015; Huganir and Nicoll, 2013). Also, the endocytic clathrin machinery is potentially involved in bridging the myosin to AMPARs, as it interacts with both GluA2 and a specific splice isoform of myosin VI (Man et al., 2000; Wollscheid et al., 2016). Myosin VI is reported to affect AMPAR trafficking in hippocampal neurons in different ways. In absence of MYO6, CME-dependent internalization of GluA1 following AMPAR stimulation is impaired (Osterweil et al., 2005). Moreover, forced recruitment of myosin VI to

AMPAR-carrying recycling endosomes leads to their transport out of dendritic spines (Esteves da Silva et al., 2015). Finally, it has been suggested that myosin VI, via its interaction with βSAP97, is important for AMPAR cell surface delivery (Nash et al., 2010).

Together, these findings raise several questions: (1) is myosin VI required for synaptic plasticity in the form of CME-dependent LTD of AMPAR-mediated synaptic transmission? (2) Is the myosin also needed for activity-dependent endocytosis of GluA2, and is it directly involved or rather acting via promoting synaptic development or other upstream events? (3) What are the molecular interactions by which myosin VI regulates synaptic AMPAR levels in an activity-dependent manner?

Here, we address these questions by studying the cerebellum, one of the brain regions where *Myo6* is expressed (Osterweil et al., 2005). Within the cerebellum, Purkinje cells (PCs) are the central neuronal signal integrators and, as such, are crucial for motor coordination, language, and social cognition (Galliano et al., 2018; Ito, 2001; Sokolov et al., 2017). PCs provide the sole output from the cerebellar cortex and receive excitatory input from parallel fibers (PFs) and climbing fibers (CFs) (Ito, 2001). LTD at PF-PC synapses is mediated by CME of GluA2-containing AMPARs and triggered by a signaling cascade involving metabotropic glutamate receptor (mGluR1) and PKC-dependent phosphorylation of GluA2 (Chung et al., 2003; Matsuda et al., 2000; Steinberg et al., 2006; Wang and Linden, 2000).

RESULTS

Myosin VI Is Present in PC Spines and Bergmann Glia Processes

To elucidate the role of myosin VI in cerebellum, we co-immunostained mouse cerebellar sections using antibodies against MYO6 (Wollscheid et al., 2016) and calbindin-D-28K to label PCs. MYO6 was present throughout the cerebellar cortex, including the molecular layer (ML) (Figure 1A). As control, we used *Snell's waltzer* mice (referred to as $Myo6^{sv/sv}$) homozygous for a recessive *Myo6* loss-of-function allele (Avraham et al., 1995; Deol and Green, 1966; Figure S1A). Western blot of $Myo6^{sv/sv}$ cerebellar extracts confirmed the absence of full-length MYO6 (Figure S1B). Immunostaining of $Myo6^{sv/sv}$ cerebellar sections using MYO6 antibody verified antibody specificity (Figure 1A). Next, we examined the ML in more detail using triple staining for MYO6, calbindin-D-28K, and VGLUT1, a marker for PF synaptic terminals. MYO6 was localized at PC dendritic spines, with only marginal signal overlap at VGLUT1-positive presynaptic terminals (Figure 1B). MYO6 also hardly overlapped with VGLUT2, a marker for CF synaptic terminals (Figure S1C), indicating that MYO6 is not predominantly presynaptic at PF- and CF-PC synapses. Immunoelectron microscopy (EM) showed that MYO6 localizes within dendritic spines of the ML and on tubulo-vesicular clusters in perisynaptic processes of Bergmann glia (Bg) cells that ensheathe the PC spines (Figures 1C and S1F–S1H). To independently confirm the myosin's localization, we observed $Myo6^{sv/sv}$ PCs expressing GFP-tagged MYO6 either lacking (GFP-MYO6-SI) or comprising the alternatively spliced large insert (GFP-MYO6-LI-SI). Both variants were significantly enriched in spines relative to dendrite shafts (Figures 1D and 1E). Moreover, MYO6 lacking the cargo-binding domain (CBD), but not GFP alone, also was enriched in spines (Figures 1D and 1E; GFP-MYO6ΔCBD, GFP). Thus, myosin VI localizes to PC spines, and its spine accumulation is independent of the CBD.

Acute Inhibition of Myosin VI Blocks LTD of AMPAR-Mediated Currents at PF-PC Synapses

LTD at PF-PC synapses depends on CME of GluA2-containing AMPARs (Wang and Linden, 2000), and myosin VI is important for CME in several cell types, including hippocampal neurons (Osterweil et al., 2005). Thus, we examined whether PF-PC LTD in cerebellar slices depends on myosin VI. PF stimulation paired with PC depolarization to induce LTD of AMPAR-mediated excitatory postsynaptic currents (EPSCs) in PCs led to robust LTD at wild-type (WT) synapses. In contrast, LTD was significantly impaired at $Myo6^{sv/sv}$ PF-PC synapses (Figure 2A). To ask whether LTD impairment is due to a dominant-negative effect of truncated MYO6 that might still be produced from the *sv* allele, we examined slices of heterozygous $Myo6^{sv/+}$ mice. However, PF-PC LTD in $Myo6^{sv/+}$ slices was indistinguishable from WT (Figure 2A), ruling out a dominant-negative effect of *sv* on LTD.

We then assessed whether impaired LTD in $Myo6^{sv/sv}$ cerebellum reflects an acute requirement of myosin VI for synaptic plasticity or whether it is an indirect consequence of a developmental deficit. Visualization of PF and CF terminals did not expose gross morphological deficits of excitatory input into $Myo6^{sv/sv}$ PCs (Figures S1D and S1E). In contrast, LTD experiments performed on WT cerebellar slices in the presence of the myosin VI inhibitor 2,4,6-triiodophenol (TIP) (Heissler et al., 2012) revealed a striking impairment of PF-PC LTD (Figure 2B). TIP did not lead to an additional impairment of LTD when applied to $Myo6^{sv/sv}$ slices (Figure 2C), demonstrating that the effect of TIP on LTD is myosin VI dependent. Of note, when compared to LTD induced in absence of DMSO, the presence of vehicle led to stronger LTD in $Myo6^{sv/sv}$, but not in WT (Figures 2A–2C). Control experiments excluded an effect of TIP on membrane resistance and basal EPSC amplitudes in WT and $Myo6^{sv/sv}$ (Figures S2A–S2K). Moreover, paired-pulse facilitation of PF synapses, a measure of presynaptic function, was not altered by TIP (Figures S2F–S2J).

To determine whether also basal synaptic transmission is affected in $Myo6^{sv/sv}$ PCs, we measured spontaneous AMPAR-mediated miniature EPSCs (mEPSCs) from cultured PCs (Figure S2L). However, compared to WT, $Myo6^{sv/sv}$ PCs exhibited comparable mEPSCs peak amplitude and inter-event interval (Figure 2D). Moreover, we observed no deficits in terms of overall morphology, dendrite length, and spine density of cultured $Myo6^{sv/sv}$ PCs (Figures S2M–S2O). We therefore conclude that basal synaptic transmission remains normal upon myosin depletion and inhibition, whereas LTD of AMPAR-mediated synaptic transmission at PF-PC synapses acutely requires myosin VI.

Myosin VI Mediates Removal of SEP-GluA2 from the Spine Surface of Cultured PCs upon cLTD

Because removal of synaptic GluA2-containing AMPARs leads to PF-PC LTD (Huganir and Nicoll, 2013), the requirement of

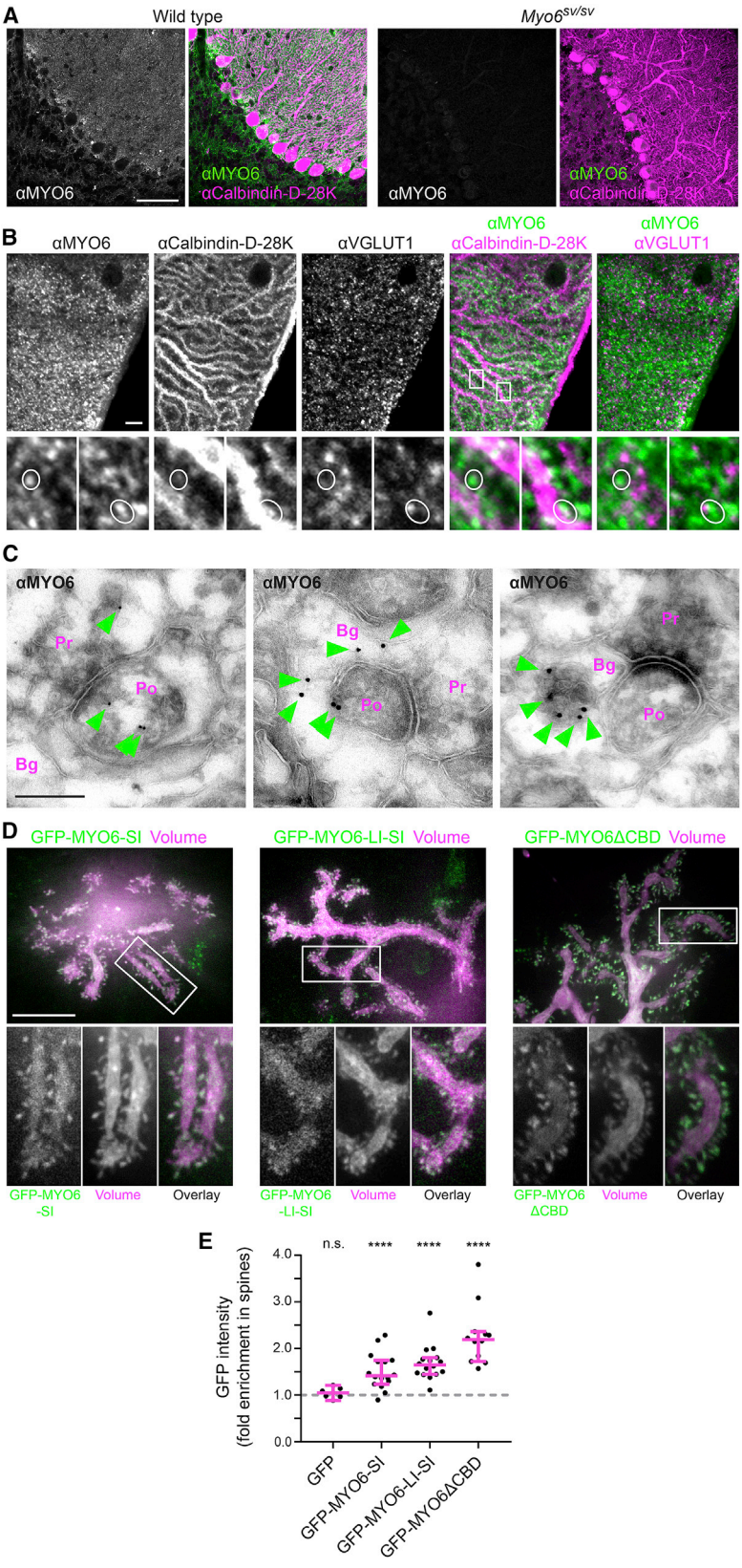

Figure 1. Myosin VI Sub-cellular Localization in the Cerebellum

(A) Confocal images of cerebellar sections from littermate control (wild-type) and *Myo6*$^{sv/sv}$ mice, immunofluorescently labeled with αMYO6 (SP1296) and αcalbindin-D-28K antibodies. Scale bar, 50 μm.

(B) Confocal images of WT cerebellar molecular layer immunofluorescently labeled with αMYO6 (SP1296), αcalbindin-D-28K, and αVGLUT1 antibodies. Scale bar, 5 μm. Bottom panels: magnifications of boxed regions in αMYO6 αcalbindin-D-28K panel are shown. White ovals: examples of spines overlapped by MYO6 are shown.

(C) EM images of cerebellar molecular layer sections labeled with αMYO6 (SP1295) and 10 nm gold coupled secondary antibodies (green arrowheads). Bg, Bergmann glia; Po, postsynapse; Pr, presynapse. Scale bar, 250 nm.

(D) Spinning disk confocal images of cultured live *Myo6*$^{sv/sv}$ PCs co-transfected with PC-specific expression plasmids p*L7-FusionRed* (volume marker) and p*L7-mGFP-Myo6-SI*, p*L7-mGFP-Myo6-LI-SI*, or p*L7-mGFP-Myo6ΔCBD*. Bottom panels: magnifications of top panels are shown. Scale bar, 20 μm.

(E) Quantification of GFP fluorescence intensity enrichment in spines relative to dendrite shafts of the PCs described in (D). WT PCs expressing GFP and FusionRed were analyzed as negative control. Magenta: median ± 95% confidence interval (CI); data points represent analyzed PCs. One sample t test against 1.0-fold enrichment shows significant difference for each GFP-MYO6 construct ($p < 0.0001$), but not for GFP alone ($p = 0.3127$).

See also Figure S1.

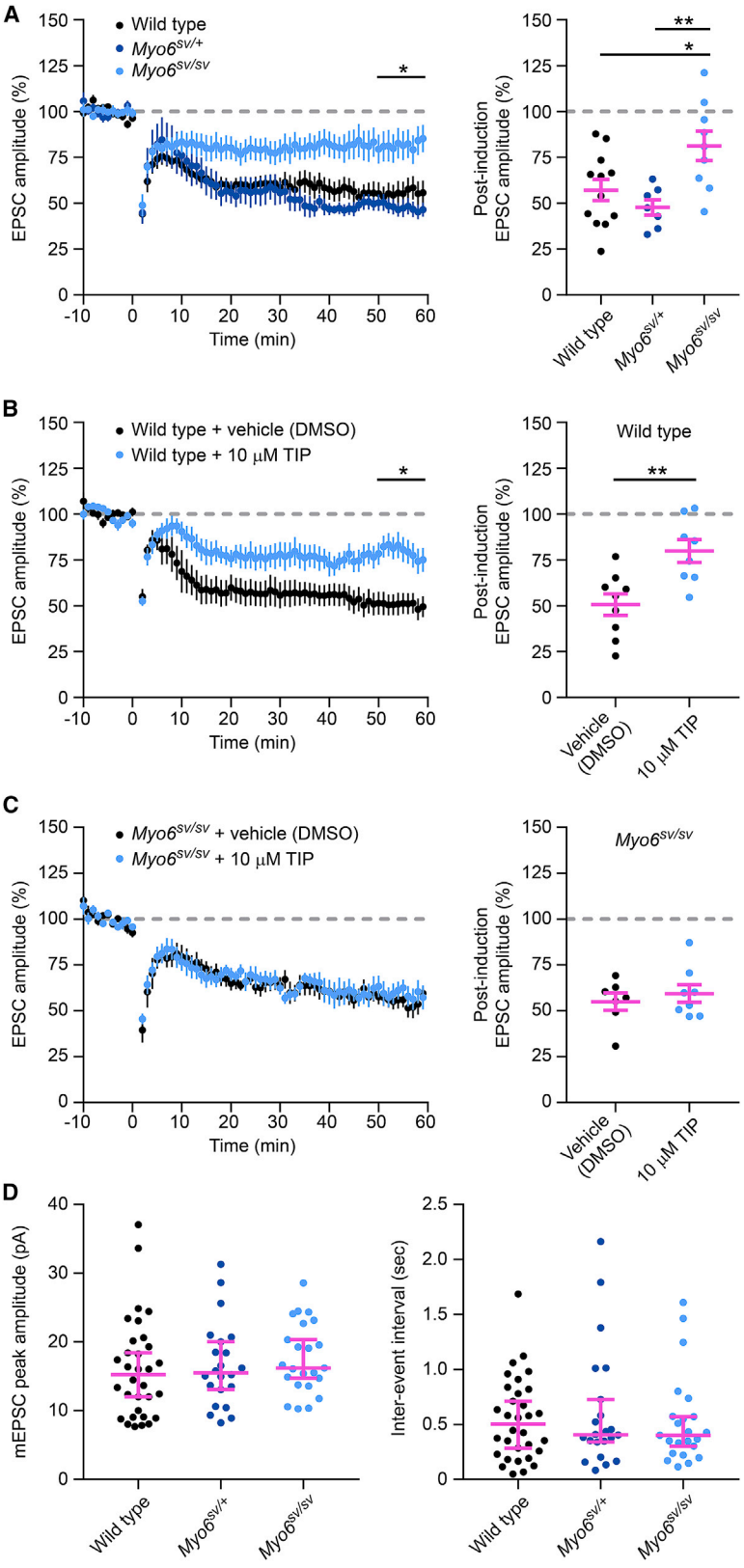

Figure 2. Acute Inhibition of Myosin VI Blocks LTD of AMPAR-Mediated Currents at PF-PC Synapses

(A) Amplitudes of PF-evoked EPSCs in PCs of acute *Myo6*$^{sv/sv}$, *Myo6*$^{sv/+}$, and WT cerebellar slices. (Left graph) Means of relative EPSC amplitudes ± SEM before and after stimulation of PFs paired with depolarization of the PC to 0 mV are shown (90× at 1 Hz at t = 0 min). (Right graph) Post-induction EPSC amplitudes at 50–60 min normalized to −10 to 0 min relative to paired stimulation are shown (magenta: mean ± SEM; data points represent analyzed PCs). Paired stimulation led to robust LTD of EPSCs in WT (n = 12) and heterozygous *Myo6*$^{sv/+}$ PCs (n = 7). Significantly less LTD was observed in *Myo6*$^{sv/sv}$ PCs (n = 9); p = 0.037, one-way ANOVA; WT versus *Myo6*$^{sv/sv}$: p = 0.0269; *Myo6*$^{sv/+}$ versus *Myo6*$^{sv/sv}$: p = 0.007; Tukey's post hoc test.

(B) Amplitudes of PF-evoked EPSCs in PCs of WT cerebellar slices exposed to TIP or vehicle. Significantly less LTD of EPSC amplitudes in presence of 10 μM TIP (n = 8) compared to vehicle are shown (0.01% DMSO; n = 9); p = 0.004, Student's t test.

(C) Amplitudes of PF-evoked EPSCs in PCs of *Myo6*$^{sv/sv}$ cerebellar slices exposed to TIP or vehicle. No significant difference in LTD in *Myo6*$^{sv/sv}$ PCs exposed to 10 μM TIP (n = 8) compared to vehicle is shown (0.01% DMSO; n = 7); p = 0.52; Student's t test.

(D) Peak amplitudes and inter-event interval of AMPAR-mediated mEPSCs in cultured *Myo6*$^{sv/sv}$, *Myo6*$^{sv/+}$, and WT PCs. Magenta: median ± 95% CI; data points represent analyzed PCs. No significant differences between genotypes for mEPSC peak amplitudes (p = 0.3772) and inter-event interval are shown (p = 0.8916); Kruskal-Wallis tests.

See also Figure S2.

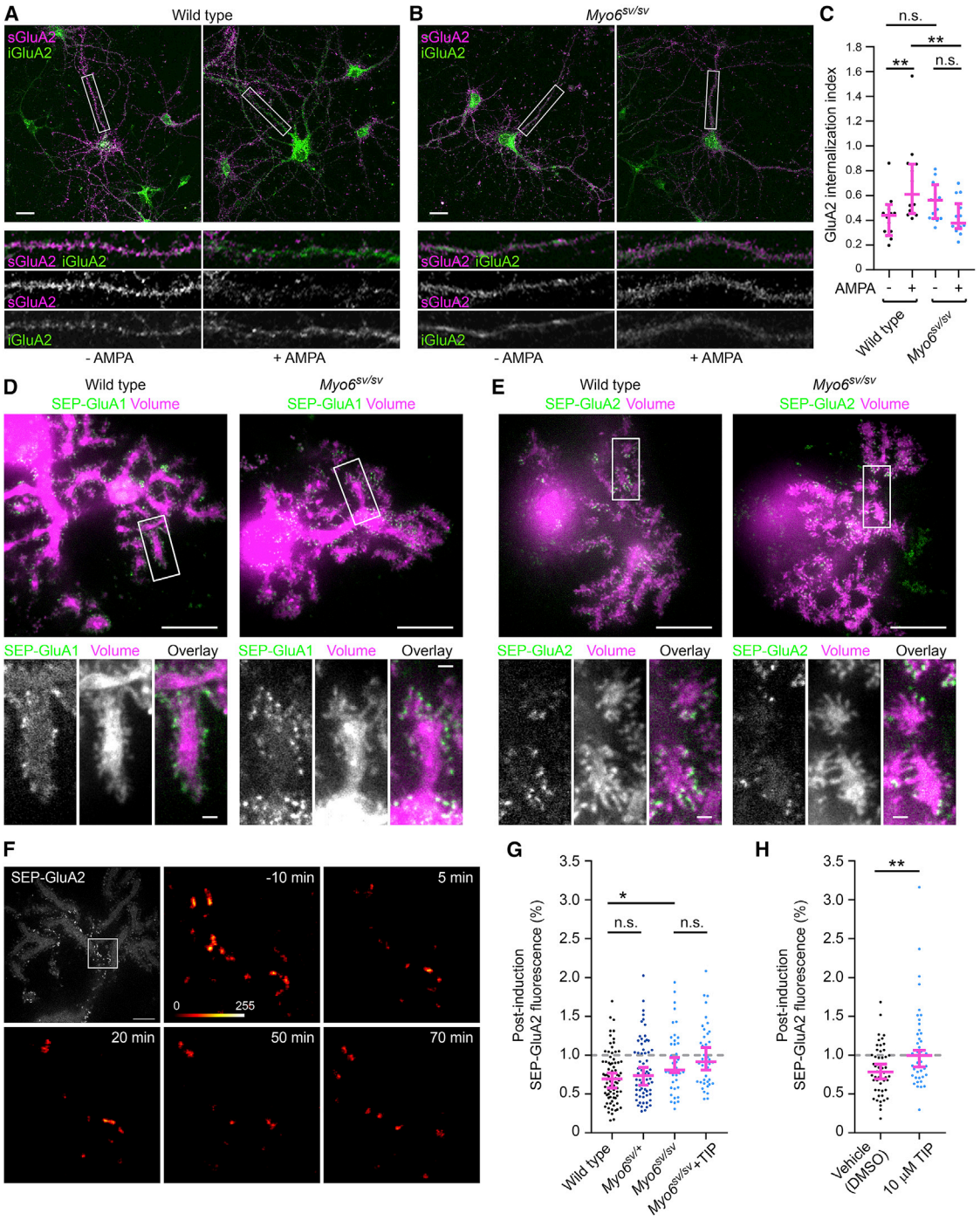

Figure 3. Myosin VI Mediates Removal of SEP-GluA2 from the Spine Surface of Cultured PCs upon cLTD

(A–C) Antibody uptake assay. Confocal images of WT (A) and *Myo6*$^{sv/sv}$ (B) hippocampal neurons, incubated with αGluA2 antibody and treated with 100 μM AMPA for 10 min (+*AMPA*) or mock-treated (−*AMPA*) are shown. Shown are surface GluA2 (*sGluA2*) and internalized GluA2 (*iGluA2*). Scale bars, 20 μm. Graph in (C) depicts internalization index; magenta: median ± 95% CI; data points represent analyzed cells. p = 0.0031, Kruskal-Wallis test; WT−AMPA versus WT+AMPA, p = 0.0088; *Myo6*$^{sv/sv}$−AMPA versus *Myo6*$^{sv/sv}$+AMPA, p = 0.2283; WT−AMPA versus *Myo6*$^{sv/sv}$−AMPA: p = 0.2461; WT+AMPA versus *Myo6*$^{sv/sv}$+AMPA: p = 0.0074; Dunn's multiple comparisons test.

(D and E) Spinning disk confocal images of live WT and *Myo6*$^{sv/sv}$ PCs transfected with p*L7-mCherry* (*volume*) and p*L7-SEP-GluA1* (D) or p*L7-SEP-GluA2* (E). Bottom panels: magnification of boxed regions is shown. Scale bars, 20 μm (top panels) and 2 μm (bottom panels).

(F) SEP-GluA2 fluorescence on PC spines diminishes after DHPG and AMPA treatment. (Top row, left panel) Spinning disk confocal image of SEP-GluA2 in a WT PC is shown. Scale bar, 10 μm. Cultures were exposed to 100 μM DHPG and 100 μM AMPA for 15 min. Panels with false-color-coded images depict boxed region at the indicated time points before and after start of DHPG and AMPA treatment.

(legend continued on next page)

myosin VI for PF-PC LTD suggests that the myosin is important for endocytic uptake of GluA2 following induction of plasticity. Therefore, we measured GluA2 internalization in cultured hippocampal neurons (Figures 3A–3C). Under basal conditions, the GluA2 internalization index was similar in *Myo6*$^{sv/sv}$ and WT neurons, indicating that GluA2 endocytosis is not impaired. However, following stimulation of AMPAR CME using AMPA (Man et al., 2000), the GluA2 internalization index increased significantly in WT, but not in *Myo6*$^{sv/sv}$ cells. Thus, myosin VI is important specifically for activity-induced endocytosis of GluA2-containing AMPARs, but not for their endocytosis under basal conditions.

To test whether myosin VI regulates AMPAR localization in PCs, we visualized surface-exposed AMPARs via super-ecliptic pHluorin (SEP)-tagged GluA1 and GluA2 (Kopec et al., 2006). Compared to volume marker, both SEP-GluA1 and SEP-GluA2 fluorescence was enriched at spines of cultured WT and *Myo6*$^{sv/sv}$ PCs (Figures 3D and 3E), indicating that the myosin is not essential for accumulating surface-exposed AMPARs on PC spines. Notably, fluorescence recovery after photobleaching (FRAP) measurements indicated increased mobility of GluA1-containing AMPARs on the spine surface of *Myo6*$^{sv/sv}$ PCs (Figures S3A–S3C).

Exposure to the mGluR1/5 agonist (S)-3,5-dihydroxyphenylglycine (DHPG) and glutamate leads to LTD of AMPAR-mediated mEPSCs in PCs of dissociated cultures (Smith-Hicks et al., 2010). Thus, we similarly exposed SEP-GluA2-expressing, cultured PCs to DHPG and AMPA to determine whether myosin VI is needed for surface GluA2 downregulation at spines following plasticity-inducing stimulation (Figures 3F–3H). Application of DHPG and AMPA for 15 min led to the depression of SEP-GluA2 spine signal of WT PCs as monitored 75 min after treatment start, indicating a persistent downregulation of SEP-GluA2 at the spine surface (Figures 3F and 3G). In contrast, the same stimulation led to significantly less depression of SEP-GluA2 signal on *Myo6*$^{sv/sv}$ PC spines (Figure 3G). As in case of PF-PC LTD, SEP-GluA2 downregulation at the spine surface of heterozygous *Myo6*$^{sv/+}$ PCs did not significantly differ from WT (Figure 3G), ruling out that the SEP-GluA2 downregulation deficit is due to a dominant-negative effect of *sv*. Because PCs were co-cultured with untransfected WT cerebellar cells, this assay only reveals phenotypes that are likely PC intrinsic (i.e., not suppressed by the presence of WT cells). We conclude that GluA2 removal from the surface of PC spines, following chemically induced LTD (cLTD) stimulation, depends on myosin VI.

The impairment in SEP-GluA2 removal in *Myo6*$^{sv/sv}$ PCs could be an indirect consequence of a deficit in synaptic or neuronal development. To directly test this, we acutely applied the myosin VI inhibitor TIP during AMPA and DHPG treatment. Compared to vehicle, TIP significantly impaired SEP-GluA2 downregulation at the spine surface of WT PCs (Figure 3H). Notably, this effect depends on myosin VI, as TIP did not significantly affect SEP-GluA2 removal in *Myo6*$^{sv/sv}$ PCs (Figure 3G). Therefore, acute inhibition of myosin VI disrupts removal of GluA2-containing AMPARs from the PC spine surface following cLTD induction.

Interaction of Myosin VI with GluA2 and α-Adaptin Increases during cLTD

We next examined the underlying mechanism by which myosin VI promotes LTD. Enrichment and turnover of filamentous actin in spines was normal in *Myo6*$^{sv/sv}$ PCs (Figures S4A–S4C), suggesting that the LTD impairment is not due to an aberrant actin cytoskeleton. We then performed a quantitative co-immunoprecipitation (coIP) assay to determine whether neuronal stimulation changes the molecular interactions of myosin VI (Figures 4A and 4B). Toward this end, acute cerebellar slices were exposed to AMPA and DHPG for 15 min to induce cLTD, followed by immunoprecipitation of MYO6. The amount of GluA2 bound to MYO6 significantly increased 30 and 60 min after start of AMPA and DHPG treatment, compared to basal conditions (Figures 4A and 4B). Importantly, this indicates that the myosin acts at the level of AMPARs during cLTD, not merely in an upstream signaling cascade. Candidates for bridging myosin VI to AMPARs include βSAP97, GRIP1, and the clathrin machinery. To dissect which of these interactions is most relevant for LTD, their ability to coIP with MYO6 was assessed. We used α-adaptin, a component of the AP-2 clathrin adaptor complex, as a specific marker for the endocytic clathrin machinery (Canagarajah et al., 2013). Strikingly, the amount of α-adaptin that coIPs with MYO6 significantly increased 30 and 60 min after the start of AMPA and DHPG treatment (Figures 4A and 4B). In contrast, the amount of GRIP1 or βSAP97 did not increase but showed a significant decrease in case of βSAP97 at 60 min after cLTD induction (Figures 4A and 4B). Therefore, our data suggest an important role specifically for the interaction of myosin VI with GluA2-containing AMPARs and the CME machinery during LTD.

To examine whether myosin VI-α-adaptin interactions take place within PCs, we employed super-resolution microscopy of cultured PCs expressing GFP-tagged MYO6. Analysis of co-localization between α-adaptin and the GFP-MYO6-LI-SI splice isoform revealed significantly increased overlap in PCs following cLTD stimulation (Figures 4C and 4D). MYO6-LI-SI comprises the alternatively spliced large insert (LI), which enables MYO6 to interact with the CME machinery. Conversely, MYO6 lacking LI does not bind clathrin (Wollscheid et al., 2016). Therefore, to test whether the increase in myosin VI-α-adaptin co-localization depends on the myosin's ability to bind the CME machinery, we analyzed cells expressing GFP-MYO6-SI, lacking LI. No increase in co-localization of α-adaptin was observed for this splice

(G) WT, *Myo6*$^{sv/+}$, and *Myo6*$^{sv/sv}$ PCs expressing SEP-GluA2 were exposed to DHPG and AMPA as in (F). In addition, *Myo6*$^{sv/sv}$ PCs were exposed to DHPG and AMPA and 10 μM TIP for 15 min. Depicted is post-induction SEP-GluA2 fluorescence on spines at 75 min after treatment start, normalized to values at 10 min before treatment start. Magenta: median ± 95% CI; data points represent analyzed PCs. $p = 0.0012$, Kruskal-Wallis test; WT versus *Myo6*$^{sv/+}$: $p = 0.5793$; WT versus *Myo6*$^{sv/sv}$: $p = 0.0234$; *Myo6*$^{sv/sv}$ versus *Myo6*$^{sv/sv}$+TIP: $p > 0.9999$; Dunn's multiple comparisons test.

(H) WT PCs expressing SEP-GluA2 were exposed to DHPG and AMPA and 10 μM TIP or vehicle (0.1% DMSO) for 15 min. Depicted is post-induction SEP-GluA2 fluorescence on spines as in (G). Magenta: median ± 95% CI; data points represent analyzed PCs; $p = 0.0027$; Mann-Whitney test.

See also Figure S3.

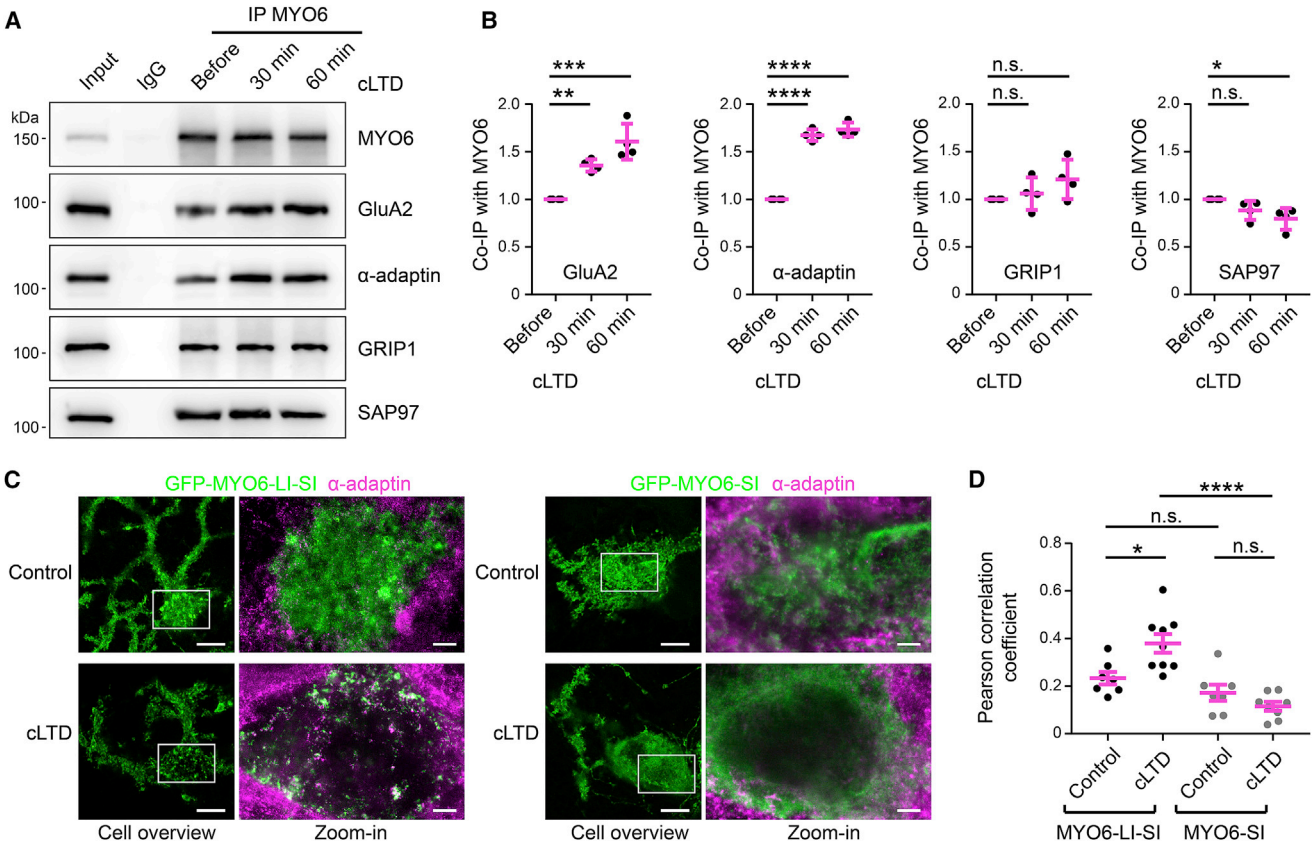

Figure 4. Interaction of Myosin VI with GluA2 and α-Adaptin Increases during cLTD

(A and B) MYO6 immunoprecipitation from acute cerebellar slices before and 30 and 60 min after cLTD induction (DHPG and AMPA, 100 μM each, for 15 min). The amount of GluA2, α-adaptin, GRIP1, and SAP97 that coIPs with MYO6 was determined by western blot analysis (A); control: non-immune immunoglobulin G (IgG). n = 4 experiments. Graphs in (B) depict quantification of coIP/MYO6 binding ratios for the indicated proteins before and 30 and 60 min after cLTD induction. Magenta: mean ± SEM; data points represent experiments. GluA2: $p = 0.0001$, $p = 0.0045$, $p = 0.0001$; α-adaptin: $p < 0.0001$, $p < 0.0001$, $p < 0.0001$; GRIP1: $p = 0.1975$, $p = 0.8445$, $p = 0.1882$; SAP97: $p = 0.0286$, $p = 0.2056$, $p = 0.0234$ (one-way ANOVA; Tukey's multiple comparisons tests before versus 30 min and before versus 60 min, respectively).

(C and D) Cultured PCs transfected with p*L7-mGFP-Myo6-LI-SI* or p*L7-mGFP-Myo6-SI* were exposed to DHPG and AMPA (100 μM each) for 15 min (*cLTD*) or mock-treated (*control*), fixed 30 min post treatment start, and stained using αGFP nanobodies and α-adaptin antibodies.

(C) Super-resolution (stimulated emission depletion [STED]) microscopy images of PCs; white indicates overlap. Scale bars, 10 μm (left panels) and 2 μm (right panels).

(D) Quantification of co-localization (Pearson's correlation coefficient) of α-adaptin with MYO6-LI-SI or MYO6-SI, measured from STED images. Magenta: mean ± SEM; data points represent analyzed PCs. $p < 0.0001$, one-way ANOVA; MYO6-LI-SI control versus MYO6-LI-SI cLTD: $p = 0.0106$; MYO6-LI-SI control versus MYO6-SI control: $p = 0.5930$; MYO6-SI control versus MYO6-SI cLTD: $p = 0.6279$; MYO6-LI-SI cLTD versus MYO6-SI cLTD: $p < 0.0001$; Sidak's multiple comparisons test.

See also Figure S4.

isoform following cLTD induction (Figures 4C and 4D). Thus, the increased myosin VI-α-adaptin co-localization following cLTD depends on the myosin's ability to bind to the CME machinery.

DISCUSSION

Here, we reveal that LTD of AMPAR-mediated synaptic transmission at cerebellar PF-PC synapses requires the unique actin-based cytoskeletal motor myosin VI. Moreover, we show that the myosin is acutely required for PF-PC LTD and directly involved in activity-dependent CME of GluA2-containing AMPARs in PCs. This defines myosin VI as a critical player of the postsynaptic machinery that mediates plasticity-related neurotransmitter receptor trafficking. Although presynaptic roles for myosin VI have been described (Hayashida et al., 2015; Yano et al., 2006), our findings did not hint on a presynaptic deficit as the origin of the impaired LTD at PF-PC synapses.

Myosin VI is known to regulate distinct membrane trafficking steps, including exo- and endocytosis. This multi-functionality is made possible, in part, by the ability of myosin VI to bind specific cargo adaptors (Tumbarello et al., 2013). βSAP97, GRIP1, and clathrin-AP-2 are known to interact with both myosin VI and AMPARs (Lv et al., 2015; Wollscheid et al., 2016; Wu et al., 2002) and thus might serve as myosin-cargo adaptors in AMPAR trafficking. In particular, it has been proposed that βSAP97-myosin VI interaction promotes AMPAR cell surface

targeting (Nash et al., 2010). Indeed, the reduction of this interaction after cLTD induction suggests a role for it under basal activity. Nonetheless, we found that myosin VI does not significantly affect synaptic AMPAR levels in PCs under basal activity.

GRIP1 is involved in dendritic transport of GluA2-containing AMPARs and their synaptic targeting (Huganir and Nicoll, 2013; Heisler et al., 2014). Because GRIP1 and its homolog GRIP2 are required for PF-PC LTD (Takamiya et al., 2008), a MYO6-GRIP1 complex might contribute to LTD, even though we did not detect a significant change in complex formation upon cLTD stimulation. In contrast, the same stimulation led to a clear increase of MYO6 interactions with GluA2 and the AP-2 component α-adaptin. AP-2 is specifically required for CME, but not other clathrin-mediated trafficking steps, and it binds to GluA2 (Lee et al., 2002; McMahon and Boucrot, 2011).

We made use of the fact that alternative splicing of the myosin VI heavy chain regulates the interaction with the clathrin machinery, including AP-2 (Wollscheid et al., 2016). Two sites in MYO6 are subject to alternative splicing (Buss et al., 2001). Presence of the small insert (SI) in the CBD allows the myosin to be recruited to secretory granules and to regulate their cortical tethering (Tomatis et al., 2013). In contrast, the LI is inserted immediately preceding the CBD and generates a clathrin machinery interaction domain (Wollscheid et al., 2016). Notably, all four MYO6 splice variants (no insert, LI, SI, and LI+SI) occur in brain (Heidrych et al., 2009). We found that LI is necessary for the cLTD-dependent increase in co-localization of MYO6 with α-adaptin in PCs. Together, our data suggest that the myosin VI interaction with the endocytic clathrin machinery is mechanistically important for LTD in PCs.

The specific requirement of myosin VI for plasticity-related AMPAR trafficking, but not for the regulation of synaptic AMPAR levels during basal activity, might be due to the fact that CME is required for activity-induced internalization of AMPARs (Man et al., 2000; Wang and Linden, 2000), but not for their constitutive endocytosis (Glebov et al., 2015). Together, our findings support a model where myosin VI facilitates PF-PC LTD via driving CME of AMPARs in PCs. Because myosin VI is regulated by calcium (Batters et al., 2016), these results open up new possibilities of how postsynaptic calcium signaling may induce PF-PC LTD.

STAR★METHODS

Detailed methods are provided in the online version of this paper and include the following:

- KEY RESOURCES TABLE
- LEAD CONTACT AND MATERIALS AVAILABILITY
- EXPERIMENTAL MODEL AND SUBJECT DETAILS
  - Mouse lines and animal care
  - Primary cell cultures
- METHOD DETAILS
  - DNA constructs
  - Genotyping
  - Neuronal cell culture
  - Antibody application details
  - Western blot of Myo6$^{sv/sv}$ cerebellar extracts
  - Co-IP assay with cerebellar slices
  - Immunolabeling of cerebellar sections
  - Purkinje cell live microscopy
  - Stimulated Emission Depletion (STED) imaging
  - GluA2 antibody uptake assay
  - Electrophysiology
- QUANTIFICATION AND STATISTICAL ANALYSIS
  - Western blot analysis
  - Microscopy image processing and analyses
  - Electrophysiology data analyses
  - Statistical analyses

SUPPLEMENTAL INFORMATION

Supplemental Information can be found online at https://doi.org/10.1016/j.celrep.2019.06.005.

ACKNOWLEDGMENTS

We thank J. Kendrick-Jones for plasmids; A.V. Failla (UKE Microscopy Imaging Facility) for help with stimulated emission depletion microscopy; and E. Thies, S. Hoffmeister-Ullerich, and H. Voß for technical support. This work was supported by EU FP7 Marie Curie Integration Grant PCIG11-GA-2012-321905; by Deutsche Forschungsgemeinschaft projects FOR 2419 WA3716/1-1 (to W.W.), FOR 2419 HE8413/1-1 (to F.F.H.), and FOR 2419 KN556/11-1 and KN556/11-2 (to M.K.); by Ritz-Stiftung (to F.F.H.); and by Hamburg Landesforschungsförderung grant LFF-FV27 (to W.W. and M.K.).

AUTHOR CONTRIBUTIONS

Conceptualization, W.W. and M.K.; Methodology, all authors; Investigation and Formal Analysis, W.W., K.L., F.F.H., K.V.G., F.L.L., M.K.R., Y.P., S.H., and M.S.; Resources, S.P.; Writing – Original Draft, W.W.; Writing – Review & Editing, all authors; Funding Acquisition, W.W., F.F.H., and M.K.; Supervision, W.W., J.R.S., J.E., and M.K.

DECLARATION OF INTERESTS

The authors declare no competing interests.

Received: June 1, 2018
Revised: May 1, 2019
Accepted: May 31, 2019
Published: July 2, 2019

SUPPORTING CITATIONS

The following reference appears in the Supplemental Information: Johnson and Schell (2009).

REFERENCES

Aschenbrenner, L., Naccache, S.N., and Hasson, T. (2004). Uncoated endocytic vesicles require the unconventional myosin, Myo6, for rapid transport through actin barriers. Mol. Biol. Cell *15*, 2253–2263.

Avraham, K.B., Hasson, T., Steel, K.P., Kingsley, D.M., Russell, L.B., Moosekker, M.S., Copeland, N.G., and Jenkins, N.A. (1995). The mouse *Snell's waltzer* deafness gene encodes an unconventional myosin required for structural integrity of inner ear hair cells. Nat. Genet. *11*, 369–375.

Batters, C., Brack, D., Ellrich, H., Averbeck, B., and Veigel, C. (2016). Calcium can mobilize and activate myosin-VI. Proc. Natl. Acad. Sci. USA *113*, E1162–E1169.

Buss, F., Arden, S.D., Lindsay, M., Luzio, J.P., and Kendrick-Jones, J. (2001). Myosin VI isoform localized to clathrin-coated vesicles with a role in clathrin-mediated endocytosis. EMBO J. *20*, 3676–3684.

Canagarajah, B.J., Ren, X., Bonifacino, J.S., and Hurley, J.H. (2013). The clathrin adaptor complexes as a paradigm for membrane-associated allostery. Protein Sci. *22*, 517–529.

Choquet, D., and Triller, A. (2013). The dynamic synapse. Neuron *80*, 691–703.

Chung, H.J., Steinberg, J.P., Huganir, R.L., and Linden, D.J. (2003). Requirement of AMPA receptor GluR2 phosphorylation for cerebellar long-term depression. Science *300*, 1751–1755.

Crepel, F., and Jaillard, D. (1991). Pairing of pre- and postsynaptic activities in cerebellar Purkinje cells induces long-term changes in synaptic efficacy in vitro. J. Physiol. *432*, 123–141.

Deol, M.S., and Green, M.C. (1966). Snell's waltzer, a new mutation affecting behaviour and the inner ear in the mouse. Genet. Res. *8*, 339–345.

Esteves da Silva, M., Adrian, M., Schätzle, P., Lipka, J., Watanabe, T., Cho, S., Futai, K., Wierenga, C.J., Kapitein, L.C., and Hoogenraad, C.C. (2015). Positioning of AMPA Receptor-Containing Endosomes Regulates Synapse Architecture. Cell Rep. *13*, 933–943.

Galliano, E., Schonewille, M., Peter, S., Rutteman, M., Houtman, S., Jaarsma, D., Hoebeek, F.E., and De Zeeuw, C.I. (2018). Impact of NMDA Receptor Overexpression on Cerebellar Purkinje Cell Activity and Motor Learning. eNeuro *5*, ENEURO.0270-17.2018.

Glebov, O.O., Tigaret, C.M., Mellor, J.R., and Henley, J.M. (2015). Clathrin-independent trafficking of AMPA receptors. J. Neurosci. *35*, 4830–4836.

Groszer, M., Keays, D.A., Deacon, R.M., de Bono, J.P., Prasad-Mulcare, S., Gaub, S., Baum, M.G., French, C.A., Nicod, J., Coventry, J.A., et al. (2008). Impaired synaptic plasticity and motor learning in mice with a point mutation implicated in human speech deficits. Curr. Biol. *18*, 354–362.

Hayashida, M., Tanifuji, S., Ma, H., Murakami, N., and Mochida, S. (2015). Neural activity selects myosin IIB and VI with a specific time window in distinct dynamin isoform-mediated synaptic vesicle reuse pathways. J. Neurosci. *35*, 8901–8913.

Heidrych, P., Zimmermann, U., Kuhn, S., Franz, C., Engel, J., Duncker, S.V., Hirt, B., Pusch, C.M., Ruth, P., Pfister, M., et al. (2009). Otoferlin interacts with myosin VI: implications for maintenance of the basolateral synaptic structure of the inner hair cell. Hum. Mol. Genet. *18*, 2779–2790.

Heisler, F.F., Loebrich, S., Pechmann, Y., Maier, N., Zivkovic, A.R., Tokito, M., Hausrat, T.J., Schweizer, M., Bähring, R., Holzbaur, E.L., et al. (2011). Muskelin regulates actin filament- and microtubule-based GABA(A) receptor transport in neurons. Neuron *70*, 66–81.

Heisler, F.F., Lee, H.K., Gromova, K.V., Pechmann, Y., Schurek, B., Ruschkies, L., Schroeder, M., Schweizer, M., and Kneussel, M. (2014). GRIP1 interlinks N-cadherin and AMPA receptors at vesicles to promote combined cargo transport into dendrites. Proc. Natl. Acad. Sci. USA *111*, 5030–5035.

Heissler, S.M., Selvadurai, J., Bond, L.M., Fedorov, R., Kendrick-Jones, J., Buss, F., and Manstein, D.J. (2012). Kinetic properties and small-molecule inhibition of human myosin-6. FEBS Lett. *586*, 3208–3214.

Huganir, R.L., and Nicoll, R.A. (2013). AMPARs and synaptic plasticity: the last 25 years. Neuron *80*, 704–717.

Isaji, M., Lenartowska, M., Noguchi, T., Frank, D.J., and Miller, K.G. (2011). Myosin VI regulates actin structure specialization through conserved cargo-binding domain sites. PLoS ONE *6*, e22755.

Ito, M. (2001). Cerebellar long-term depression: characterization, signal transduction, and functional roles. Physiol. Rev. *81*, 1143–1195.

Johnson, H.W., and Schell, M.J. (2009). Neuronal IP3 3-kinase is an F-actin-bundling protein: role in dendritic targeting and regulation of spine morphology. Mol. Biol. Cell *20*, 5166–5180.

Kneussel, M., and Hausrat, T.J. (2016). Postsynaptic Neurotransmitter Receptor Reserve Pools for Synaptic Potentiation. Trends Neurosci. *39*, 170–182.

Kneussel, M., and Wagner, W. (2013). Myosin motors at neuronal synapses: drivers of membrane transport and actin dynamics. Nat. Rev. Neurosci. *14*, 233–247.

Kopec, C.D., Li, B., Wei, W., Boehm, J., and Malinow, R. (2006). Glutamate receptor exocytosis and spine enlargement during chemically induced long-term potentiation. J. Neurosci. *26*, 2000–2009.

Lee, S.H., Liu, L., Wang, Y.T., and Sheng, M. (2002). Clathrin adaptor AP2 and NSF interact with overlapping sites of GluR2 and play distinct roles in AMPA receptor trafficking and hippocampal LTD. Neuron *36*, 661–674.

Lv, K., Chen, L., Li, Y., Li, Z., Zheng, P., Liu, Y., Chen, J., and Teng, J. (2015). Trip6 promotes dendritic morphogenesis through dephosphorylated GRIP1-dependent myosin VI and F-actin organization. J. Neurosci. *35*, 2559–2571.

Majewski, Ł., Sobczak, M., Havrylov, S., Jóźwiak, J., and Rędowicz, M.J. (2012). Dock7: a GEF for Rho-family GTPases and a novel myosin VI-binding partner in neuronal PC12 cells. Biochem. Cell Biol. *90*, 565–574.

Man, H.Y., Lin, J.W., Ju, W.H., Ahmadian, G., Liu, L., Becker, L.E., Sheng, M., and Wang, Y.T. (2000). Regulation of AMPA receptor-mediated synaptic transmission by clathrin-dependent receptor internalization. Neuron *25*, 649–662.

Masters, T.A., Tumbarello, D.A., Chibalina, M.V., and Buss, F. (2017). MYO6 Regulates Spatial Organization of Signaling Endosomes Driving AKT Activation and Actin Dynamics. Cell Rep. *19*, 2088–2101.

Matsuda, S., Launey, T., Mikawa, S., and Hirai, H. (2000). Disruption of AMPA receptor GluR2 clusters following long-term depression induction in cerebellar Purkinje neurons. EMBO J. *19*, 2765–2774.

McMahon, H.T., and Boucrot, E. (2011). Molecular mechanism and physiological functions of clathrin-mediated endocytosis. Nat. Rev. Mol. Cell Biol. *12*, 517–533.

Nash, J.E., Appleby, V.J., Corrêa, S.A., Wu, H., Fitzjohn, S.M., Garner, C.C., Collingridge, G.L., and Molnár, E. (2010). Disruption of the interaction between myosin VI and SAP97 is associated with a reduction in the number of AMPARs at hippocampal synapses. J. Neurochem. *112*, 677–690.

Oberdick, J., Smeyne, R.J., Mann, J.R., Zackson, S., and Morgan, J.I. (1990). A promoter that drives transgene expression in cerebellar Purkinje and retinal bipolar neurons. Science *248*, 223–226.

Osterweil, E., Wells, D.G., and Mooseker, M.S. (2005). A role for myosin VI in postsynaptic structure and glutamate receptor endocytosis. J. Cell Biol. *168*, 329–338.

Schindelin, J., Arganda-Carreras, I., Frise, E., Kaynig, V., Longair, M., Pietzsch, T., Preibisch, S., Rueden, C., Saalfeld, S., Schmid, B., et al. (2012). Fiji: an open-source platform for biological-image analysis. Nat. Methods *9*, 676–682.

Shemiakina, I.I., Ermakova, G.V., Cranfill, P.J., Baird, M.A., Evans, R.A., Souslova, E.A., Staroverov, D.B., Gorokhovatsky, A.Y., Putintseva, E.V., Gorodnicheva, T.V., et al. (2012). A monomeric red fluorescent protein with low cytotoxicity. Nat. Commun. *3*, 1204.

Slot, J.W., and Geuze, H.J. (2007). Cryosectioning and immunolabeling. Nat. Protoc. *2*, 2480–2491.

Smith-Hicks, C., Xiao, B., Deng, R., Ji, Y., Zhao, X., Shepherd, J.D., Posern, G., Kuhl, D., Huganir, R.L., Ginty, D.D., et al. (2010). SRF binding to SRE 6.9 in the Arc promoter is essential for LTD in cultured Purkinje cells. Nat. Neurosci. *13*, 1082–1089.

Sokolov, A.A., Miall, R.C., and Ivry, R.B. (2017). The Cerebellum: Adaptive Prediction for Movement and Cognition. Trends Cogn. Sci. *21*, 313–332.

Spudich, J.A., and Sivaramakrishnan, S. (2010). Myosin VI: an innovative motor that challenged the swinging lever arm hypothesis. Nat. Rev. Mol. Cell Biol. *11*, 128–137.

Spudich, G., Chibalina, M.V., Au, J.S., Arden, S.D., Buss, F., and Kendrick-Jones, J. (2007). Myosin VI targeting to clathrin-coated structures and dimerization is mediated by binding to Disabled-2 and PtdIns(4,5)P2. Nat. Cell Biol. *9*, 176–183.

Steinberg, J.P., Takamiya, K., Shen, Y., Xia, J., Rubio, M.E., Yu, S., Jin, W., Thomas, G.M., Linden, D.J., and Huganir, R.L. (2006). Targeted in vivo mutations of the AMPA receptor subunit GluR2 and its interacting protein PICK1 eliminate cerebellar long-term depression. Neuron *49*, 845–860.

Takamiya, K., Mao, L., Huganir, R.L., and Linden, D.J. (2008). The glutamate receptor-interacting protein family of GluR2-binding proteins is required for

long-term synaptic depression expression in cerebellar Purkinje cells. J. Neurosci. *28*, 5752–5755.

Tomatis, V.M., Papadopulos, A., Malintan, N.T., Martin, S., Wallis, T., Gormal, R.S., Kendrick-Jones, J., Buss, F., and Meunier, F.A. (2013). Myosin VI small insert isoform maintains exocytosis by tethering secretory granules to the cortical actin. J. Cell Biol. *200*, 301–320.

Tumbarello, D.A., Kendrick-Jones, J., and Buss, F. (2013). Myosin VI and its cargo adaptors - linking endocytosis and autophagy. J. Cell Sci. *126*, 2561–2570.

Wagner, W., Brenowitz, S.D., and Hammer, J.A., 3rd. (2011a). Myosin-Va transports the endoplasmic reticulum into the dendritic spines of Purkinje neurons. Nat. Cell Biol. *13*, 40–48.

Wagner, W., McCroskery, S., and Hammer, J.A., 3rd. (2011b). An efficient method for the long-term and specific expression of exogenous cDNAs in cultured Purkinje neurons. J. Neurosci. Methods *200*, 95–105.

Wang, Y.T., and Linden, D.J. (2000). Expression of cerebellar long-term depression requires postsynaptic clathrin-mediated endocytosis. Neuron *25*, 635–647.

Wells, A.L., Lin, A.W., Chen, L.Q., Safer, D., Cain, S.M., Hasson, T., Carragher, B.O., Milligan, R.A., and Sweeney, H.L. (1999). Myosin VI is an actin-based motor that moves backwards. Nature *401*, 505–508.

Wollscheid, H.P., Biancospino, M., He, F., Magistrati, E., Molteni, E., Lupia, M., Soffientini, P., Rottner, K., Cavallaro, U., Pozzoli, U., et al. (2016). Diverse functions of myosin VI elucidated by an isoform-specific α-helix domain. Nat. Struct. Mol. Biol. *23*, 300–308.

Wu, H., Nash, J.E., Zamorano, P., and Garner, C.C. (2002). Interaction of SAP97 with minus-end-directed actin motor myosin VI. Implications for AMPA receptor trafficking. J. Biol. Chem. *277*, 30928–30934.

Yano, H., Ninan, I., Zhang, H., Milner, T.A., Arancio, O., and Chao, M.V. (2006). BDNF-mediated neurotransmission relies upon a myosin VI motor complex. Nat. Neurosci. *9*, 1009–1018.

STAR★METHODS

KEY RESOURCES TABLE

REAGENT or RESOURCE	SOURCE	IDENTIFIER
Antibodies		
Rabbit anti-MYO6 (SP1295/1296)	Wollscheid et al., 2016	N/A
Rabbit anti-MYO6 (clone H-215)	Santa Cruz	Cat#sc-50461; RRID: AB_2148617
Rabbit anti-MYO6 (clone KA15)	Sigma-Aldrich	Cat#M5187; RRID: AB_260563
Mouse anti-α-Tubulin (clone DM1A)	Sigma-Aldrich	Cat#T9026; RRID: AB_477593
Mouse anti-Calbindin-D-28K	Sigma-Aldrich	Cat#C9848; RRID: AB_476894
Rabbit anti-Calbindin-D-28K	Merck Millipore	Cat#AB1778; RRID: AB_2068336
Guinea pig anti-VGLUT1	Merck Millipore	Cat#AB5905; RRID: AB_2301751
Guinea pig anti-VGLUT2	Merck Millipore	Cat#AB2251-I; RRID: AB_2665454
Mouse monoclonal anti-Glutamate Receptor 2, extracellular (clone 6C4)	Merck Millipore	Cat#MAB397; RRID: AB_2113875
Mouse anti-α-Adaptin (clone 8)	BD Biosciences	Cat#610502; RRID: AB_397868
Mouse anti-α-Adaptin (clone AP6)	Abcam	Cat#ab2730; RRID: AB_303255
Rabbit anti-SAP97	Synaptic Systems	Cat#124 302; RRID: AB_2092022
Mouse anti-GRIP1 (clone32/GRIP)	BD Biosciences	Cat#611319; RRID: AB_398845
Camelid anti-GFP nanobody (clone 1H1) conjugated to Atto647N	Synaptic Systems/NanoTag Biotechnologies	Cat#N0301-At647N; RRID: AB_2744620
Donkey anti-mouse peroxidase conjugated	Jackson ImmunoResearch	Cat#715-036-151; RRID: AB_2340774
Donkey anti-rabbit peroxidase conjugated	Jackson ImmunoResearch	Cat#711-036-152; RRID: AB_2340590
Donkey anti-rabbit Cy3 conjugated	Jackson ImmunoResearch	Cat#711-166-152; RRID: AB_2313568
Donkey anti-mouse Cy3 conjugated	Jackson ImmunoResearch	Cat#715-165-150; RRID: AB_2340813
Donkey anti-mouse Alexa Fluor 488 conjugated	Jackson ImmunoResearch	Cat#715-486-151; RRID: AB_2572300
Goat anti-mouse peroxidase-conjugated light chain-specific	Jackson ImmunoResearch	Cat#115-035-174; RRID: AB_2338512
Donkey anti-guinea pig Cy5 conjugated	Jackson ImmunoResearch	Cat#706-175-148; RRID: AB_2340462
Goat anti-mouse Alexa Fluor 594 conjugated	BioLegend	Cat#405326; RRID: AB_2563308
Chemicals, Peptides, and Recombinant Proteins		
(S)-AMPA	Tocris	Cat#0254
D-AP5	Tocris	Cat#0106
(+)-bicuculline	Tocris	Cat#0130
(-)-bicuculline methiodide	Tocris	Cat# 0131
Complete protease inhibitor tablets	Sigma-Aldrich/Roche	Cat#04693116001
(S)-3,5-DHPG	Abcam	Cat#ab120007
DNase I	Sigma-Aldrich/Roche	Cat#04716728001
Fetal bovine serum	Thermo Fisher Scientific/GIBCO	Cat#10082139
Papain	Sigma-Aldrich	Cat#P3125
Proteinase K	Sigma-Aldrich/Roche	Cat#03115828001
Taq DNA Polymerase	Sigma-Aldrich/Roche	Cat#04728874001
2,4,6-triiodophenol (TIP)	Sigma-Aldrich	Cat#19566
2,4,6-triiodophenol (TIP)	Sigma-Aldrich	Cat#137723
Tetrodotoxin citrate (TTX)	Alomone Labs	Cat#T-550
Triton X-100	Sigma-Aldrich/Roche	Cat#11332481001
Critical Commercial Assays		
Antigen Retrieval Reagent	R&D Systems	Cat#CTS013
Aqua-Poly/Mount	Polysciences	Cat#18606-20

(*Continued on next page*)

Continued

REAGENT or RESOURCE	SOURCE	IDENTIFIER
Dynabeads Protein G	Thermo Fisher Scientific/Invitrogen	Cat#10003D
Hibernate-E	Thermo Fisher Scientific/GIBCO	Cat#A1247601
Immobilon-P PVDF Membrane	Merck Millipore	Cat#IPVH00010
Immobilon HRP Substrate	Merck Millipore	Cat#WBKLS0500
Mouse Neuron Nucleofector Kit	Lonza	Cat# VPG-1001
QuickExtract	Epicenter	Cat#QE09050
Tissue-Tek O.C.T Compound	Sakura Finetek	Cat#4583
Experimental Models: Organisms/Strains		
Mouse: B6 x STOCK *Tyr*$^{c\text{-}ch}$ *Bmp5*^{se} +/+ *Myo6*^{sv}/J (*Myo6*$^{sv/sv}$)	The Jackson Laboratory	Stock No: 000578
Oligonucleotides		
SV1: 5′-CTGACCCTGATCACTTAGCAGAGTTG-3′	This study	N/A
SV2: 5′-CATTGGGCCAGGTCACAGAAGTAAGC-3′	This study	N/A
SV3: 5′-GGTCCTCTGAAAGAGTAACC-3′	This study	N/A
WW_M6FL_fw: 5′-TGTACTACTAGTGAAGATGGA AAGCCCGTTTGGGCACC-3′	This study	N/A
WW_M6STOP_rv: 5′-TACACTGTCGACCTACTTG AGCAGGTTCTGCAGCATGG-3′	This study	N/A
WW_SpeI_LNK_fw: 5′-GCACTTAGATCTACTAG TGGCCGGCCATAGACGCGTGTCGACTCATGG-3′	This study	N/A
Recombinant DNA		
Plasmid: p*L7-mGFP*	Wagner et al., 2011a	N/A
Plasmid: p*L7-mCherry*	Wagner et al., 2011a	N/A
Plasmid: p*L7-mGFP-F-tractin* (p*L7-ITPKA-9-52–mGFP*)	Wagner et al., 2011a	N/A
Plasmid: p*L7-FusionRed*	This study	N/A
Plasmid: pFusionRed-C	Evrogen	Cat#FP411
Plasmid: p*L7-mGFP-2*	This study	N/A
Plasmid: p*L7-FusionRed-2*	This study	N/A
Plasmid: p*L7-mGFP-Myo6-SI*	This study	N/A
Plasmid: p*L7-mGFP-Myo6-LI-SI*	This study	N/A
Plasmid: p*L7-mGFP-Myo6*ΔCBD	This study	N/A
Plasmid: p*L7-mGFP-actin*	This study	N/A
Plasmid: pPA-TagRFP-actin	Evrogen	Cat#FP813
Plasmid: pCI-SEP-GluR1	Kopec et al., 2006	RRID: Addgene_24000
Plasmid: pCI-SEP-GluR2(R)	Kopec et al., 2006	RRID: Addgene_24001
Plasmid: p*L7-SEP-GluR1*	This study	N/A
Plasmid: p*L7-SEP-GluR2*	This study	N/A
Software and Algorithms		
Software: Clampfit 10.7	Molecular Devices	https://www.moleculardevices.com
Software: Fiji	Schindelin et al., 2012	http://fiji.sc
Software: Igor Pro	WaveMetrics	https://www.wavemetrics.com
Software: ImageJ 1.38	National Institutes of Health	https://imagej.nih.gov
Software: MetaMorph 7.1	Molecular Devices	https://www.moleculardevices.com
Software: Patchmaster	HEKA	http://www.heka.com
Software: Prism 7.04	GraphPad Software	https://www.graphpad.com
Other		
Glass bottom dish	Invitro Scientific	Cat#D35-14-1.5-N

LEAD CONTACT AND MATERIALS AVAILABILITY

Further information can be obtained from and requests for reagents may be directed to and will be fulfilled by the Lead Contact, Matthias Kneussel (matthias.kneussel@zmnh.uni-hamburg.de).

EXPERIMENTAL MODEL AND SUBJECT DETAILS

Mouse lines and animal care

The study was carried out in accordance with the recommendations of the European Community Council Directive (2010/63/EU) in accordance with German and EU laws, and the procedures used were approved by the City of Hamburg (Behörde für Gesundheit und Verbraucherschutz, Lebensmittelsicherheit und Veterinärwesen). We used B6 x STOCK *Tyr*$^{c\text{-}ch}$ *Bmp5*^{se} +/+ *Myo6*^{sv}/J mice that were obtained from The Jackson Laboratory (stock no. 000578) and that were repeatedly backcrossed to C57BL/6J WT mice, thereby yielding mice that lack *Tyr*$^{c\text{-}ch}$ and *Bmp5*^{se} alleles, but carry the *Snell's waltzer* (*Myo6*^{sv}) allele that leads to a premature stop codon in *Myo6* shortly after the myosin motor domain (Deol and Green, 1966; Avraham et al., 1995). Homozygous *Myo6*$^{sv/sv}$ (*Snell's waltzer*), heterozygous *Myo6*$^{sv/+}$, and wild-type (WT; *Myo6*$^{+/+}$) littermates were obtained by mating *Myo6*$^{sv/+}$ mice to each other. Genotypes were determined from DNA obtained from tail biopsies. Mice were maintained in a pathogen-free, temperature- and humidity-controlled vivarium on a 12 h light/dark schedule. Mice had access to standard laboratory chow and water *ad libitum*. Both male and female mice were included in the experiments. The age of mice was chosen in accordance with the scientific question and is specified in the Method Details section.

Primary cell cultures

Primary dissociated cultures of neurons were prepared as described in Method Details and maintained in an incubator at 37°C, with 5% CO_2 and saturated humidity. Brains from pups of both sexes were used since *Myo6*^{sv} is an autosomal recessive allele that disrupts *Myo6* expression in both males and females.

METHOD DETAILS

DNA constructs

Prefix 'p*L7*' denotes plasmids carrying the PC-specific *L7* (*Pcp-2*) promoter (Oberdick et al., 1990). Plasmids p*L7-mGFP*, p*L7-mCherry* and p*L7-mGFP-F-tractin* (i.e., p*L7-ITPKA-9-52–mGFP*) were described previously (Wagner et al., 2011a; Wagner et al., 2011b). To generate p*L7-FusionRed* for expressing a red fluorescent volume marker in PCs, the FusionRed ORF (Shemiakina et al., 2012) was released from pFusionRed-C vector (#FP411, Evrogen, RU) using NheI, BglII restriction enzymes and ligated with the vector backbone obtained by NheI, BglII digest of p*L7-mGFP*. A version of p*L7-mGFP*, termed p*L7-mGFP-2*, carrying a modified multiple cloning site was created by replacing the 18 base pair (bp) BglII, SalI fragment in p*L7-mGFP* with a fragment generated by BglII, SalI digestion of annealed oligonucleotides WW_SpeI_LNK_fw (5′-GCACTTAGATCTACTAGTGGCCGGCCAT AGACGCGTGTCGACTCATGG-3′) and its reverse complement. Similarly, p*L7-FusionRed-2* was generated by replacing the NcoI, BglII fragment in p*L7-mGFP-2* that contains mGFP with a fragment comprising FusionRed released from p*L7-FusionRed* via NcoI, BglII digest. Plasmid p*L7-mGFP-Myo6-SI* encodes the full-length MYO6 splice isoform comprising the small insert (SI), fused to the C terminus of mGFP. It carries a PCR-generated fragment corresponding to the *Myo6* ORF of GenBank: NM_001039546.2, amplified from mouse brain cDNA using oligonucleotide primers WW_M6FL_fw (5′-TGTACTACTAGTGAAGATGGAAAGCC CGTTTGGGCACC-3′) and WW_M6STOP_rv (5′-TACACTGTCGACCTACTTGAGCAGGTTCTGCAGCATGG-3′). The PCR fragment was digested with SpeI and SalI, and ligated with SpeI, SalI-digested p*L7-mGFP-2* backbone. Plasmid p*L7-mGFP-Myo6-LI-SI* encodes the MYO6 splice isoform containing both large insert (LI) and SI. It carries the *Myo6* ORF as in GenBank: XM_006510835.3 and corresponds to p*L7-mGFP-Myo6-SI* with a 227 bp DraIII, BssHII-fragment (harbors the LI insertion site) being replaced by a synthesized 323 bp DraIII, BssHII-fragment containing LI (Eurofins, GER). To create a plasmid encoding MYO6 lacking the CBD, a SphI, SalI fragment in p*L7-mGFP-Myo6-SI* was replaced by a synthesized SphI, SalI fragment encoding the C-terminal part of MYO6 without the CBD (i.e., residues following amino acids VQATKAAAGT... being replaced by AAAPVRKLA-Stop). Plasmid p*L7-mGFP-actin* was created by inserting a BglII, BamHI fragment encoding human β-actin from pPA-TagRFP-actin (#FP813, Evrogen, RU) in proper orientation into the BglII-site of p*L7-mGFP*. To create p*L7-SEP-GluA1*, a fragment encoding SEP-tagged GluA1 was released by NaeI, SalI digestion from pCI-SEP-GluR1 (gift from Robert Malinow; Addgene #24000; Kopec et al., 2006) and ligated with NotI (blunted) and SalI-digested backbone of p*L7* (Wagner et al., 2011b). Similarly, p*L7-SEP-GluA2* was generated by ligating the same digested p*L7* backbone with a fragment encoding SEP-tagged GluA2 from pCI-SEP-GluR2(R) (gift from Robert Malinow; Addgene #24001; Kopec et al., 2006) modified to encode GluA2- instead of GluA1-signal petide.

Genotyping

Genotypes were determined via PCR using genomic DNA obtained by digesting tissue biopsies with QuickExtract DNA Extraction Solution (Epicenter) following the manufacturer's instructions. Alternatively, biopsies were digested using Protease K lysis buffer (10 mM Tris-HCl pH 8.5, 50 mM KCl, 2.5 mM EDTA, 0.45% [v/v] IPEGAL, 0.45% [v/v] Tween20, and 0.1 mg/ml Protease K [#03115828001, Roche]) for 30 min at 65°C, followed by incubation for 2 min at 97°C. To discriminate between WT, homo- and

heterozygous carriers of the *Myo6*^{sv} allele, PCR was performed using primers SV1 (5′-CTGACCCTGATCACTTAGCAGAGTTG-3′), SV2 (5′-CATTGGGCCAGGTCACAGAAGTAAGC-3′), and SV3 (5′-GGTCCTCTGAAAGAGTAACC-3′), Taq DNA Polymerase (#04728874001, Roche), and reaction conditions of 94°C for 2 min; 35 times (94°C for 10 s, 54°C for 30 s, 72°C for 19 s); and 72°C for 5 min. DNA fragments were separated on 0.8 – 1.5% agarose gels and imaged using a UV transillumination/digital camera system (INTAS Science Imaging Instruments). The *Myo6*^{sv} allele yields a 318 bp fragment, the WT allele yields a 230 bp fragment (Figure S1A).

Neuronal cell culture

Dissociated cerebellar cultures

Preparation and transfection of dissociated cerebellar cultures containing Purkinje cells was done as described (Wagner et al., 2011b), with minor modifications. Briefly, E17-18 mouse embryos were obtained from pregnant C57BL/6J WT mice, or from *Myo6*$^{sv/+}$ females mated to *Myo6*$^{sv/+}$ males, after euthanization with CO_2 and cervical dislocation. Embryonic brains were isolated in ice-cold modified Hank's balanced salt solution (MHS; GIBCO 14170088, Thermo Fisher Scientific) and were stored in Hibernate-E medium (GIBCO A1247601, Thermo Fisher Scientific) for several hours while performing PCR genotyping on embryo head tissue DNA, if necessary. The cerebellar primordium was minced and digested for 20 min at 30°C using 7 U papain (P3125, Sigma-Aldrich). After addition of heat-inactivated fetal bovine serum (FBS; GIBCO 10082139, Thermo Fisher Scientific), cells were triturated in MHS containing 12 mM $MgSO_4$ (M2643, Sigma-Aldrich) and 5 U/ml DNase I (Roche 04716728001, Sigma-Aldrich) and filtered through a nylon mesh (180 μm pore size, #NY8H04700, Millipore). After a wash in MHS, all cells from one cerebellum were nucleofected in a single reaction using Mouse Neuron Nucleofector® Kit (VPG-1001; Lonza, CH; nucleofection program O-003) according to the manufacturer's protocol. Transfected cells from *Myo6*$^{+/+}$ or *Myo6*$^{sv/sv}$ embryos were then mixed with untransfected cells from one WT cerebellum resuspended in 300 μl DFM [Dulbecco's Modified Eagle's Medium/Nutrient Mixture F-12 Ham (D6434, Sigma-Aldrich) supplemented with 1x GlutaMAX (GIBCO 35050-038; Thermo Fisher Scientific), 100 μM putrescine dihydrochloride (P5780, Sigma-Aldrich), 30 nM Na_2SeO_3 (S5261, Sigma-Aldrich), 40 nM progesterone (P7556, Sigma-Aldrich), 0.77 nM L-3,3′,5-tri-iodothyronine (T2877, Sigma-Aldrich), 2 μM cytosine β-D-arabinofuranoside (C6645, Sigma-Aldrich), 200 μg/ml apo-transferrin (T1147, Sigma-Aldrich), 100 μg/ml BSA (A3156, Sigma-Aldrich), and 20 μg/ml insulin (I0516; Sigma-Aldrich)] containing 10% (*v/v*) FBS. The entire mixture (cells from a transfected and an untransfected cerebellum) was plated into the well of a single glass bottom dish (D35-14-1.5-N, Invitro Scientific) coated with poly-L-ornithine hydrobromide (P4638, Sigma-Aldrich). At 1.5 h after plating, 1.8 mL DFM containing 5 μg/ml gentamicin (GIBCO 15710049; Thermo Fisher Scientific) were added per dish, and 4 - 36 h after plating 1.5 mL of culture medium were replaced with fresh DFM/gentamicin. Subsequently 1 mL of medium was replaced by fresh DFM/gentamicin every week. Cultured neurons were analyzed after 12-18 days *in vitro* (DIV).

Dissociated hippocampal cultures

Hippocampal neuron cultures were prepared from E17-18 mouse embryos as described (Heisler et al., 2011) by seeding 80,000 cells onto 12 mm coverslips coated with 5 μg/ml poly-L-lysine in phosphate-buffered saline (PBS). Before dissociation, embryonic brains were stored in Hibernate-E medium (GIBCO A1247601, Thermo Fisher Scientific) for several hours while performing genotyping of DNA obtained from embryo head tissue. Cells were cultured in Clonetics PNGM Primary Neuron Growth Medium (Lonza, CH) and analyzed at 14 DIV.

Antibody application details

Primary antibodies

WB indicates dilution used for western blot, IHC indicates dilution used for immunohistochemistry, STED indicates dilution used for STED, and IP indicates amount used per immunoprecipitation. αMYO6 (rabbit SP1295/SP1296; IHC 1:200; Wollscheid et al., 2016), αMYO6 (rabbit, H-215, sc-50461, Santa Cruz; WB 1:200; antibody was pre-adsorbed against acetone powder prepared from *Snell's waltzer* brain and used 1:20 for IHC), αMYO6 (rabbit, KA15, M5187, Sigma-Aldrich, IP 4 μg), α-alpha-Tubulin (mouse, clone DM1A; T9026; Sigma-Aldrich; WB 1:5,000), αCalbindin-D-28K (mouse, clone CB-955, C9848, Sigma-Aldrich; IHC 1:300), αCalbindin-D-28K (rabbit, AB1778, Merck Millipore; IHC 1:100), αVGLUT1 (guinea pig, AB5905, Merck Millipore; IHC 1:5,000), αVGLUT2 (guinea pig, AB2251, Merck Millipore; IHC 1:5,000), αGluA2 (mouse, clone 6C4, MAB397, Merck Millipore; WB 1:1,000), αalpha-adaptin (mouse, clone 8, 610502, BD Biosciences, WB 1:1,000), αalpha-adaptin (mouse, clone AP6, ab2730, Abcam, STED, 1:200), αSAP97 (rabbit, 124302, Synaptic Systems, WB: 1:1,000), αGRIP1 (mouse, clone 32/GRIP, 611319, BD Biosciences, WB 1:1,000), and αGFP nanobody conjugated to Atto647N (camelid, clone 1H1, N0301-At647N, Synaptic Systems/NanoTag Biotechnologies; STED, 1:200).

Secondary antibodies

Purchased from Jackson ImmunoResearch, if not indicated otherwise, and used at a dilution of 1:15,000 for WB, 1:500 for IHC, and 1:200 for STED. α-mouse HRP (#715-036-151), α-rabbit HRP (#711-036-152), α-rabbit Cy3 (#711-166-152), α-mouse Cy3 (#715-165-150), α-mouse Alexa Fluor 488 (#715-486-151), α-guinea pig Cy5 (#706-176-148), and α-mouse Alexa Fluor 594 (405326, BioLegend).

Western blot of Myo6$^{sv/sv}$ cerebellar extracts

Cerebella of 4 - 7 month old mice were lysed in IMAC buffer (in mM: 20 HEPES, 100 potassium acetate, 40 KCl, 5 EGTA, 5 $MgCl_2$, pH 7.2) comprising 1% Triton X-100 and protease inhibitors (cOmplete tablets, Roche #04 693 116 001) by drawing into a 1 mL

syringe (5 x with 21G cannula, 8 x with 26G cannula). The homogenate was incubated on ice for 30 min before centrifugation for 5 min at 1,000 x g, 4°C. The supernatant was mixed with 5 x SDS-loading buffer (10% SDS, 50% glycerol, 250 mM Tris pH 6.8, 500 mM DTT, 0.05% bromophenol blue), boiled (5 min, 95°C), separated via SDS-PAGE using 10% gels, and blotted onto Immobilon-P PVDF membranes (#IPVH00010, Merck Millipore). The indicated primary and suitable horse-radish peroxidase-coupled secondary antibodies were used. Chemiluminiscence detection was performed using Immobilon Western HRP Substrate (#WBKLS0500, Merck Millipore) and ChemoCam Imager ECL Typ HR 16-3200 (INTAS Science Imaging Instruments, Göttingen, Germany).

Co-IP assay with cerebellar slices

Cerebella of 22 - 24 week old adult mice (one cerebellum per IP sample) were dissected in ice-cold dissection buffer (in mM: 240 sucrose, 2.5 Na_2HPO_4, 2 $MgSO_4$, 26 $NaHCO_3$, 10 glucose, 1 $CaCl_2$) and 400 μm thick cerebellar slices were prepared using a tissue chopper (H. Saur, GER). Slices were allowed to recover for 1 h in chambers containing artificial cerebrospinal fluid (ACSF; in mM: 124 $NaCl_2$, 5 KCl, 1.25 Na_2HPO_4, 2 $MgSO_4$, 26 $NaHCO_3$, 20 glucose, 2 $CaCl_2$, bubbled with 5% CO_2 and 95% O_2, pH 7.4 at room temperature [RT]). Slices were then left untreated (time point "Before") or treated for 15 min with ACSF containing 100 μM (S)-3,5-DHPG (ab120007, Abcam) and 100 μM (S)-AMPA (#0254, Tocris) for cLTD induction. Treated slices were then transferred to regular ACSF and allowed to recover for 15 (time point 30 min) and 45 min (time point 60 min). Subsequently, homogenization of cerebellar slices was carried out with 26G and 20G cannulas in 500 μl homogenization buffer (in mM: 20 HEPES, 100 KCl, 5 EGTA, 5 $MgCl_2$, pH 7.2) containing 1% Triton X-100 and freshly added protease inhibitors (cOmplete tablets, Roche #04 693 116 001), 5 mM DTT and 1 mM PMSF (Sigma-Aldrich). Homogenates were incubated for 30 min on ice followed by 5 min centrifugation at 1,000 x g and supernatants were collected for immunoprecipitation. Before, Dynabeads Protein G (Thermo Fisher Scientific/Invitrogen; 30 μl per sample) were washed 3 times with PBS and incubated with 4 μg of the immunoprecipitation antibody (αMYO6, rabbit, clone KA15, M5187, Sigma-Aldrich) in PBS overnight at 4°C. Unbound antibody was removed by washing 3 times with homogenization buffer prior to incubation with cerebellar slice homogenates on a rotation-wheel overnight at 4°C. Beads were then washed 5 times for 5 min with IP buffer (in mM: 50 NaCl, 50 Tris pH 7.5, 5 $MgCl_2$) containing 1% Triton X-100 on a rotation-wheel. Samples were analyzed by SDS-PAGE and western blotting using the indicated antibodies. Images were acquired using the ChemoCam Imager ECL Typ HR 16-3200 (INTAS Science Imaging Instruments, Göttingen, Germany).

Immunolabeling of cerebellar sections

Immunoelectron microscopy

Adult mice were deeply anesthetized by a mixture of ketanest and rompun and transcardially perfused with 4% paraformaldehyde (PFA) (w/v) and 0.1% glutaraldehyde (w/v) in phosphate buffer (PB). 150 μm vibratome sections of the brain were cut. After washing in PBS pH 7.2, sections were treated with 0.3% H_2O_2 and 1% $NaBH_4$ in PBS for 30 min to inhibit endogenous peroxidase activity. After rinsing in PBS, sections were incubated with 10% horse serum (PS) containing 0.2% bovine serum albumin (BSA) for 15 min to block nonspecific binding sites, and incubated with the specific αMYO6 (SP1295) antibody diluted 1:1,000 in PBS containing 1% PS and 0.2% BSA over night. Sections were washed with PBS, then incubated with biotinylated goat anti-rabbit IgG (Vector Laboratories, CA) diluted 1:1,000 in carrier for 90 min. After rinsing, sections were incubated with ABC (Vector Laboratories, CA) diluted 1:100 in PBS for 90 min. Sections were washed in PBS and reacted in diaminobenzidine (DAB)-H_20_2 solution (Sigma-Aldrich) for 10 min. Sections were either mounted on glass coverslips for light microscopic observation or dehydrated and embedded after fixation with 1% osmiumtetroxide (w/v) in Epon (Carl Roth GmbH & Co. KG, Germany). For postembedding immunogold labeling, small pieces of cryoprotected cerebellar tissue (2.3 M sucrose) were mounted on specimen holders immersed in liquid nitrogen and ultrathin sections (70 nm) were cut and labeled according to Slot and Geuze (2007). Briefly, sections were collected on Carbon-Formvar-coated nickel grids (Science Services GmbH, Germany). αMYO6 (SP1295) antibody was used diluted 1:100 and recognized with 10 nm large protein A gold secondary antibody (G. Posthuma, University Medical Center Utrecht). Ultrathin sections were examined in an EM902 (Zeiss, Germany). Pictures were taken with a TRS 2K digital camera (A. Tröndle, Germany). *Myo6*$^{sv/sv}$ sections were used as negative control.

Immunofluorescence microscopy

Adult mice (age 5 – 8 months) were transcardially perfused with 4% PFA in PBS. Brains were post-fixed in PFA/PBS (~2 h), cryoprotected overnight in PBS containing 30% sucrose. Then brains were frozen using Tissue-Tek O.C.T. Compound (Sakura Finetek, Germany) on dry ice and sectioned into 25 μm thick sagittal sections using a cryostat. Sections were mounted on glass slides and treated in 1 x Antigen Retrieval Reagent (R&D Systems #CTS013) for 4 min at 93°C, cooled down for 10 min at RT, rinsed in 0.1 M PB pH 7.3, and blocked in PB containing 5% normal donkey serum. Antibodies were diluted in PB containing 1% normal donkey serum, 1% BSA, 0.1% Triton X-100 and sections were incubated for 2 days at 4°C with gentle agitation. Sections were washed 3 times 10 min at RT with PB, incubated with fluorescently labeled secondary antibody in PB containing 1% normal donkey serum, 1% BSA, 0.1% Triton X-100 for 24 h at 4°C, washed 3 times 10 min at RT with PB, mounted on glass slides with Aqua-Poly/Mount (Polysciences, Inc., USA), and imaged on a confocal laser scanning microscope (Olympus FV1000; 60x objective; 488 nm, 559 nm, and 635 nm laser lines for excitation; Z stacks of planes with 1 μm optical thickness acquired).

Purkinje cell live microscopy

General conditions

Cultured PCs were observed using a spinning disk confocal microscope (Visitron Systems) consisting of an inverted microscope (Nikon Ti-E) equipped with a spinning disk (Yokogawa), solid state lasers (405, 488, 561 and 647 nm), a 100x objective, an EM-CCD camera (Hamamatsu Photonics), autofocus system (Nikon TI-ND6-PFS), a multi-point FRAP/photo-activation module (VisiFRAP, Visitron Systems), and an incubation chamber for controlled environmental conditions (37°C, 5% CO_2). Cerebellar cultures were imaged directly in the culture dish containing their conditioned growth medium, if not indicated otherwise.

SEP-GluA2 cLTD assay

For monitoring the effect of AMPA/DHPG on SEP-GluA2 fluorescence on PC spines (Figures 3F–3H), PCs transfected with p*L7-SEP-GluA2* and p*L7-FusionRed* were used. Medium was exchanged to Ringer solution (in mM: 135 NaCl, 5 KCl, 1 $CaCl_2$, 2 $MgCl_2$, 10 HEPES, 5 glucose, pH 7.4 with NaOH) immediately before starting the experiment. During observation, cultures were continuously perfused at a flow rate of ~0.5 ml/min at RT with Ringer, or for 15 min with Ringer containing 100 μM (S)-3,5-DHPG (ab120007, Abcam) and 100 μM (S)-AMPA (#0254, Tocris), and (if indicated) 10 μM 2,4,6-triiodophenol (TIP; #19566, Sigma-Aldrich) or vehicle (0.1% DMSO). SEP-GluA2 fluorescence was imaged every 5 min (1 s exposure time), 4 to 17 cells were followed simultaneously in an experiment.

Fluorescence recovery after photobleaching

For measuring F-actin turnover in PC spines via fluorescence recovery after photobleaching (FRAP) analysis, cultured PCs transfected with p*L7-mGFP-actin* and p*L7-FusionRed* were used. GFP-actin signal was imaged using spinning disk microscopy with a frame rate of 1/sec (500 ms exposure time). In each trial, following 5 frames of baseline recording, GFP-actin signal was bleached using 405 nm laser on 6 single spines of the same cell (circular region of 12 pixel diameter placed on each spine; total bleach time ~4 s). Imaging was resumed immediately thereafter for 145 s at 1 frame/sec. Similarly, FRAP analysis of SEP-GluA1 turnover on the PC spine surface was performed using spinning disk microscopy of cultured PCs transfected with p*L7-SEP-GluA1* and p*L7-FusionRed*. To monitor both SEP-GluA1 and spines, green and red signals were imaged throughout the experiment. Exposure times were 500 ms and 250 ms, respectively. Following 5 frames of baseline recording (5 s interval), the SEP-GluA1 signal was bleached using 405 nm laser light on up to 6 single spines of one cell, as above. Imaging was resumed immediately thereafter at 0.4 frames/min.

Stimulated Emission Depletion (STED) imaging

For STED imaging, dissociated cerebellar cultures comprising PCs transfected with p*L7-mGFP-Myo6-LI-SI* or p*L7-mGFP-Myo6-SI* were transferred to Ringer solution (control) or Ringer solution containing 100 μM (S)-3,5-DHPG (ab120007, Abcam) and 100 μM (S)-AMPA (#0254, Tocris) for 15 min at RT for cLTD induction. Cultures were then transferred to fresh Ringer solution and allowed to recover for 15 min before fixing with 4% PFA in PBS for 15 min at RT. Cells were then permeabilized and blocked for 20 min at RT using PBS containing 0.23% Triton X-100 and 10% donkey serum. After that, cells were incubated for 1 h with αGFP nanobodies conjugated to Atto647N and an antibody against α-adaptin (ab2730, Abcam, UK), followed by Alexa Fluor 594 secondary antibody. Coverslips with stained cells were mounted with TDE Abberior Mounting Medium (Abberior Instruments GmbH, GER). 2D-STED images with a pixel size of 20 nm were acquired from the stained PCs with Abberior Instruments STED microscope (Abberior Instruments GmbH, GER) using 60x P-Apo 1.4 NA oil objective. Atto 647N was excited by a 640 nm laser and depleted by a 775 nm pulsed laser, Alexa Fluor 594 was excited by 561 nm laser and depleted by 775 nm pulsed laser.

GluA2 antibody uptake assay

Antibody recognizing the GluA2 N terminus (final concentration 10 μg/ml; MAB397, Merck Millipore) was added to culture medium of live hippocampal neurons at 14 DIV. After incubation for 15 min at 37°C, (S)-AMPA (final concentration 100 μM) or vehicle (water) was added to the antibody-containing medium. After incubation for 10 min at 37°C, cells were rinsed with PBS, followed by fixation in 4% PFA/PBS for 10 min at RT. To visualize surface GluA2, the fixed cells were incubated with α-mouse Alexa Fluor 488 secondary antibody (1:200 in PBS with 1% BSA) for 1 h at RT. After that, cells were permeabilized for 8 min at RT using PBS containing 0.25% Triton X-100 and incubated with α-mouse Cy3 secondary antibody (1:200 in PBS with 1% BSA) for 1 h at RT to visualize internalized GluA2. Coverslips with stained cells were mounted with Aqua-Poly/Mount (Polysciences, USA) and imaged on a confocal laser scanning microscope (Olympus FV1000, 60x objective, single plane acquired) using identical settings for each cell.

Electrophysiology

Acute cerebellar slices

Acute cerebellar slices were prepared from 20 to 27 day-old mice as described previously (Groszer et al., 2008). Mice were decapitated under deep isoflurane anesthesia and cerebellar vermis was rapidly (< 1 min) removed and placed in ice-cold artificial cerebrospinal fluid (ACSF2; in mM: 125 NaCl, 2.5 KCl, 2 $CaCl_2$, 1 $MgCl_2$, 1.25 NaH_2PO_4, 26 $NaHCO_3$, 20 glucose, bubbled with 95%

O_2 and 5% CO_2, pH 7.4 at RT). 300 μm thick parasagittal slices were cut (VT 1200 S, Leica, Germany) and incubated in ACSF2 at 35°C for 40 min before they were stored at RT until use. Somatic whole-cell voltage-clamp recordings were obtained from visually identified PCs with an EPC-10 patch-clamp amplifier (HEKA, Germany), controlled by Patchmaster software (HEKA), and patch pipettes pulled from borosilicate glass (Hilgenberg, Germany) to reach 4 - 6 MΩ resistance when filled with intracellular solution (in mM: 145 $CsMeSO_3$, 4 NaCl, 10 HEPES, 10 TEA-Cl, 2 $MgCl_2$, 4 Mg-ATP, 0.4 Na-GTP, 0.1 EGTA, pH 7.3 adjusted with HCl). Single EPSCs were evoked at 0.1 Hz (baseline frequency) by activating PFs using a glass pipette placed in the molecular layer and stimuli (4 - 15 V, 100 μs) applied through a stimulus isolator (npi electronic, Germany). For the LTD experiments shown in Figures 2B and 2C, WT and *Myo6*$^{sv/sv}$ cerebellar slices were exposed to vehicle (0.01% DMSO) or 10 μM 2,4,6-triiodophenol (TIP; #19566, Sigma-Aldrich). To measure paired-pulse facilitation of PF synapses (paired-pulse ratio) during these experiments, paired-pulse stimulation of PFs was performed at 0.1 Hz (50 ms inter-stimulus interval; see Figures S2F–S2K). Wash in experiments were performed using 0.1% DMSO (vehicle) or 10 μM TIP (#137723, Sigma-Aldrich, Figures S2A–S2E). Series resistance (R_S) compensation was adjusted so that the remaining, uncompensated R_S value was kept constant at 12 MΩ. Recordings were performed at RT in presence of 10 μM of $GABA_A$-receptor blocker (-)-bicuculline methiodide (#0131, Tocris). After obtaining a stable baseline for at least 10 min, LTD of PF-EPSCs was induced by pairing PF stimulation with depolarizing voltage steps (to 0 mV for 100 ms; 90 times at 1 Hz, synaptic stimulation in the middle of the depolarization; Crepel and Jaillard, 1991). Then, PF stimulation was resumed at 0.1 Hz and LTD induction was monitored for 60 min. LTD was quantified as the average reduction of EPSC amplitudes at 50 to 60 min after LTD induction, normalized to the average reduction during the 10 min before induction.

Dissociated cerebellar cultures

PCs in dissociated cerebellar culture transfected with p*L7-mGFP* and pL7-*FusionRed* were identified based on GFP-fluorescence using a Zeiss Axiovert 405 M microscope. PCs were whole cell patch-clamped at 13 - 14 DIV at RT using borosilicate glass pipettes (Hilgenberg, Germany). Pipettes had a resistance of 3 - 5 MΩ when filled with intracellular solution containing (in mM: 140 K^+-gluconate, 4 $MgCl_2$, 0.5 EGTA, 10 HEPES, 4 Na_2ATP, 0.4 Na_3GTP, pH 7.3, adjusted with KOH). The extracellular solution corresponded to Ringer containing (in mM) 0.0005 TTX (T-550, Alomone Labs), 0.020 (+)-bicuculline (#0130, Tocris), and 0.050 D-AP5 (#0106, Tocris), pH 7.4, adjusted with NaOH. EPSCs were recorded at a holding potential of −70 mV with an EPC9 amplifier using Patchmaster software (HEKA).

QUANTIFICATION AND STATISTICAL ANALYSIS

Western blot analysis

To quantify relative immunoblot signals for the co-IP assay, signal intensities of protein bands were measured using ImageJ software (version 1.38, National Institutes of Health, NIH). Signal intensities were then normalized, as compared to loading control signals for immunoblots and the mean of control data points was set to 1, in order to provide easier readability.

Microscopy image processing and analyses

Processing of shown images

Confocal laser scanning and STED microscopy: Linear contrast adjustment was applied to generate the shown images. Images in Figure 1A are maximum intensity projections of four Z-planes, with images of the same channel subjected to identical contrast adjustment. Images in Figures 1B and S1C–S1E are maximum intensity projections of three and four Z-planes, respectively. Spinning disk confocal microscopy: Linear contrast adjustment and Gaussian or low-pass filters (to reduce noise) were applied to generate the shown images. Images in Figures 3D and 3E were generated by averaging three consecutively recorded images (5 s interval) to improve signal to noise ratio. Images shown in Figure S2M are Z stack maximum intensity projections.

Spine enrichment quantification

The fold enrichment of GFP-tagged myosin (Figure 1E) and F-tractin (Figure S4B) in spines of live PCs was determined from spinning disk microscopy images as follows, using Fiji image processing software (Schindelin et al., 2012): Integrated fluorescence intensity of volume and GFP was measured in a small circular region (constant dimension throughout analysis) placed either onto the spine head, at the dendritic shaft nearby, or outside the cell (to measure background). Regions were placed using the volume image (i.e., blind to the GFP signal). The respective background signals were subtracted from measured spine and dendrite intensities. To normalize for volume effects and to calculate the relative enrichment of GFP-signal (*e*) in spines compared to dendrites, the following calculation was performed with the background-corrected signals:

$$e = \frac{\mathrm{GFP(Spine)\ x\ Volume(Dendrite)}}{\mathrm{GFP(Dendrite)\ x\ Volume\ (Spine)}}$$

8-10 spine/dendrite combinations were analyzed per cell to calculate the mean fold enrichment of GFP signal in spines.

PC dendrite length

Dendrite length was determined by manually tracing dendrites of cultured PCs expressing mGFP in Z stacks comprising the whole dendritic tree using MetaMorph 7.1 (Molecular Devices).

PC spine density

Spine density was determined from single plane spinning disk confocal images of dendrites of PCs expressing mGFP using Fiji (analyzed mean dendrite length of 66 μm/cell).

SEP-GluA2 cLTD assay

The effect of AMPA/DHPG stimulation on SEP-GluA2 fluorescence on PC spines (Figures 3F–3H) was determined using Fiji by applying a median filter (1 pixel wide) to the recorded images, followed by drawing regions around all visible spines (selected via applying a threshold above dendrite background level). Total spine fluorescence intensity was measured and background intensity subtracted. Post-induction SEP-GluA2 fluorescence (75 min after start of the stimulation) was determined for each cell by normalizing to initial SEP-GluA2 fluorescence (10 min before start of stimulation).

STED imaging

Image data were analyzed by selecting regions of interest on PCs, followed by measuring Pearson's correlation coefficients between two channels of the raw STED images via Coloc2 plug-in in Fiji.

FRAP analysis of GFP-actin

GFP-actin fluorescence intensity signal in bleached spines was quantified using Fiji (Schindelin et al., 2012). Intensity was measured from a region of constant size encompassing the spine throughout the duration of the experiment. To determine recovery of the bleached fluorescence signal, the intensity measured in each frame was first reduced by the intensity remaining in the first frame after bleaching, yielding baseline-corrected intensity values F_b. To correct for overall bleaching during the experiment, F_b was multiplied with a bleach factor (y) calculated for each trial and time point, yielding bleach-corrected intensity values (F_{bc}). To obtain y, fluorescence intensity in each frame was measured from part of the cell that included only spines not targeted by FRAP bleaching. After background correction of the measured intensities, bleach factor y was determined for each time point using Excel (Microsoft) by fitting a curve described by the exponential equation

$$y = at^b$$

(*a* and *b*, fitted variables; *t*, time) to the values obtained by dividing the initial, background-corrected intensity by the background-corrected intensity at each time point. The mean of F_{bc} (the bleach-corrected intensity values) before FRAP bleaching was normalized to 100% (F_0), and F_{bc} values at each time point after bleaching were expressed relative to F_0 (GFP-actin fluorescence, % of initial), yielding the fluorescence recovery curve. For each experiment, a mean recovery curve was calculated by averaging the data of all measured spines. Only experiments with > 10 FRAPed spines were considered. To calculate plateau and time constant of GFP-actin fluorescence intensity recovery in spines, the mean recovery curves were fitted to the equation

$$y = P(1 - \exp(-kx))$$

(y, GFP-actin fluorescence intensity; x, time; P, plateau; k, inverse of τ).

FRAP analysis of SEP-GluA1

SEP signal recovery was only analyzed if presence of the spine was confirmed during the experiment by FusionRed signal. SEP fluorescence intensity of single spines was measured using Fiji before and after bleaching from a region comprising the SEP signal of a single spine and defined by thresholding the image at background level. Similar as for FRAP analysis of GFP-actin, the recovery of fluorescence intensity was determined by subtracting the intensity measured in the first frame after bleaching from the intensity measured in each frame, yielding F_b. The mean F_b of the first 5 frames was normalized to 100% (F_0), and F_b at each time point following bleaching was expressed relative to F_0. To calculate plateau and time constant of SEP fluorescence intensity recovery in spines, the mean recovery curves were fitted to the equation

$$y = P(1 - \exp(-kx))$$

(y, GFP-actin fluorescence intensity; x, time; P, plateau; k, inverse of τ).

GluA2 antibody uptake assay

To determine the GluA2 internalization index, signal intensities of surface and internalized GluA2 were measured along neurites of randomly chosen hippocampal neurons using Fiji. The internalization index was determined via dividing the background-corrected internalized GluA2 mean intensity by the background-corrected surface GluA2 mean intensity.

Electrophysiology data analyses

Acute cerebellar slices

Recordings were analyzed using Igor Pro (WaveMetrics). Slices were excluded if a sudden change in series resistance, holding current or synaptic responses occurred.

Dissociated cerebellar cultures

mEPSCs were analyzed with Clampfit 10.7 (Molecular Devices). A template was constructed to detect and determine the amplitude of mEPSCs. 100 mEPSCs were collected in each PC after visual confirmation of each mEPSC. Only those PCs were analyzed which exhibited a healthy appearance and presented vivid synaptic activity in the beginning of an experiment, while recording in extracellular solution not yet containing TTX, D-AP5 and bicuculline.

Statistical analyses

Raw values were imported into Excel (Microsoft) before statistic analyses were performed using Prism 7.04 (GraphPad Software, Inc.). The exact value of *n* is stated in the figure legends, in case it is not directly visible from the shown graph. Statistical tests used, what *n* represents, and whether mean, median, SD, SEM, confidence intervals are shown, is indicated in the figure legends. For datasets fulfilling the Shapiro-Wilk normality test, *P value*s were obtained using unpaired and two-sided Student's t test (if variance in datasets was the same according to F test) or using t test with Welch's correction (if variance in datasets was different according to F test). When comparing two groups not fulfilling the normality test, exact *P value*s were obtained using Mann-Whitney test. For comparison of more than two groups that all fulfill the normality test, presence of a significant difference was first evaluated using ordinary one-way ANOVA, followed by Dunnett's, Sidak's or Tukey's multiple multiple comparisons test, as indicated. For comparison of more than two groups where not all fulfill the normality test, presence of a significant difference was first evaluated using ordinary Kruskal-Wallis test, followed by Dunn's multiple comparisons test. Significance values are indicated in the figures as * $p < 0.05$; ** $p < 0.01$; *** $p < 0.001$; **** $p < 0.0001$; $p > 0.05$ was deemed not significant (n.s.).